DYNAMIC WIND TUNNEL LOAD AND ATTITUDE MEASUREMENTS USING

STATE ESTIMATION

A Thesis

by

KRISTA MARIE CRATTY

Submitted to the Office of Graduate and Professional Studies of
Texas A&M University
in partial fulfillment of the requirements for the degree of

MASTER OF SCIENCE

Chair of Committee,	Edward White
Committee Members,	Moble Benedict
	David Staack
Head of Department,	Rodney Bowersox

December 2017

Major Subject: Aerospace Engineering

ABSTRACT

Sting-mounted models that undergo significant unsteady motion suffer from degraded data quality because the data is time-averaged to remove the unsteady fluctuations. However, time-averaged data is not always an accurate representation of the true data. Eliminating such errors is addressed in this study by developing and evaluating the performance of a Kalman filter for estimating instantaneous load and model attitude data for a sting-mounted wind tunnel model. The particular model is 6.25% scale WB-57 that is tested in the Oran W. Nicks Low Speed Wind Tunnel at Texas A&M University. The pitch and plunge motion of the model are measured using accelerometers and the loads and moments are measured using an internal balance.

This work shows that a simplified state-space model consisting of 3 state variables and one measurement can successfully estimate plunge position and normal force of a sting-mounted test article by minimizing the difference between actual and predicted measurements in the Kalman filter. The aerodynamic normal force results compared well with conventional time-averaged wind tunnel data used as a metric to measure the successfulness of the state estimation technique.

A more extensive state space model with 6 state variables and 4 measurements has the potential to estimate the pitch position and pitching moment in conjunction with the plunge position and loads. Doing so would require a different technique to quantify and tune the process noise covariance matrix.

ACKNOWLEDGEMENTS

CONTRIBUTORS AND FUNDING SOURCES

Contributors

This work was supervised by a thesis committee consisting of Professor Ed White and Professor Moble Benedict of the Department of Aerospace Engineering and Professor David Staack of the Department of Mechanical Engineering.

All work for the thesis was completed by the student, under the advisement of Ed White of the Department of Aerospace Engineering.

Funding Sources

NOMENCLATURE

a   Lift Curve Slope

AR   Aspect Ratio

b   Wingspan

BMC   Balance Moment Center

I_{yy} mr_g^2, Pitch Moment of Inertia

g   Gravitational Acceleration

k   Reduced Frequency

m   Mass of Model

$M_{aero,BMC}$ Aerodynamic Pitching Moment about the Balance Moment Center

$M_{aero,AC}$ Aerodynamic Pitching Moment about the Aerodynamic Center

M_{IB} Internal Balance Pitching Moment

N_{aero} Normal Force due to and Measured by Internal Balance

N_{IB} Normal Force due to Aerodynamic Forces

q   Dynamic Pressure

r_g Pitch Axis Radius of Gyration about the Balance Moment Center

S   Wing Area

U_∞ Freestream Velocity

W   Weight of Model

x_{AC} Distance of Aerodynamic Center of Model with Respect to the

                Balance Moment Center

X_{CG}	Distance of Center of Gravity of Model with Respect to the Balance Moment Center
z'	Deflection in the z-direction from the Commanded Position, also referred to as the plunge position
α	Angle of Attack
ω	Frequency of Oscillations
ω_n	Natural Frequency
θ	$\theta_0 + \theta'$, True Pitch Angle of Model
θ_0	Constant Commanded Angle of Attack
θ'	Rotation of the Commanded Angle of Attack due to Unsteadiness of Model

TABLE OF CONTENTS

LIST OF FIGURES

LIST OF TABLES

CHAPTER I

INTRODUCTION AND LITERATURE REVIEW

The objective of this study is to develop and implement a Kalman filter to estimate the instantaneous position and loads of a wind tunnel model attached to the test section via a flexible sting. A Kalman filter is a mathematical model that estimates the state of a dynamical system by comparing instantaneous measurements and expected states. Using the difference between the actual measurements and expected states, the state estimates are updated [1].

While wind tunnel testing can quickly produce accurate data when models are steady, unsteady model motion can degrade data quality and impede test performance. In current practice at the Texas A&M University Low Speed Wind Tunnel (LSWT) as well as other facilities, time averages are taken of the unsteady data to eliminate the unsteady fluctuations. Data is only recorded if load fluctuations fall below a specified threshold. Then, a correction for mean sting bending is applied during data reduction. The angle of attack varies across the sample because the model is not at a true static condition. The current process is time consuming and does not address the dynamics of the model.

This thesis applies a Kalman filter to the unsteady data produced by a dynamic model mounted in the wind tunnel to effectively capture the instantaneous loads and attitude. This enables a sting mounted model to be tested more efficiently and for higher quality data to be recorded.

1

The Kalman filter combines the internal balance data and accelerometer data to provide a closer approximation to the true state of the test article than if the filter used only one sensor. Accelerometers are used to measure the linear acceleration. Using two accelerometers each mounted at separate locations both linear (plunge) and pitch acceleration can be measured. The end of the sting has an internal force balance that measures loads and moments about its balance moment center. The filter also incorporates a linearized governing equation model. The Kalman filter focuses on prediction and correction where prediction is accomplished using the model and the correction is accomplished using the measurements. This study will focus on the pitch and plunge deflections of the model and the associated normal force and pitch moment measured by the internal balance.

Conventionally, data is recorded during wind tunnel testing when the tunnel and model configuration is "on condition." In most test cases, angle of attack of the model is an important parameter that must be controlled with high accuracy when collecting data. However, an error in angle of attack of the test article is introduced by induced aerodynamic forces transmitting dynamics on a sting-mounted model [2]. These inertial effects produce a bias in the axial force [3]. The phenomenon is designated as "sting whip" by Steinle and Peters [3]. When the model and tunnel are not on condition or the article is too dynamic, the test point cannot be completed until the desired condition is met. This precludes the completion of test objectives. The importance of the current research is to be able to filter out the sting whip effect such that the data collected is

representative of the true state of the model, since at this time, there is no process in routine wind tunnel testing that compensates for this effect.

Multiple studies have been completed surrounding inefficiencies in wind tunnel testing and ways to overcome these fallbacks. Steinle and Peters focused on developing an integrated method of deriving both inertial and dynamic derivative effects from data using elastic properties of the sting/balance support system to calculate the true dynamics. Assumptions made during the test were that the sting and model forward of the internal balance were treated as a single mass, the model forward of the end of the sting was rigid, and the cantilever response of the sting bending was in phase with the applied normal force and moment due to the internal balance. The results of the wind tunnel testing concluded that "random motion a sting-model support system can induce a thrusting bias error to axial force, and hence drag, measurement." It was also concluded that there was a lack of sufficient data to expand the analysis for higher dynamic motion. Steinle and Peters analyzed one data point at Mach 0.9 and state that a missing component is changing the Mach number and dynamic pressure to investigate changes in results. Fortunately, the work presented in this thesis shows the result of the trends of varying dynamic pressure. [3]

Crawford and Finley conducted a wind tunnel test in the Langley 16-Foot Transonic Tunnel to try to correct the sting whip effect. The purpose of the test was to validate the accuracy of a sting whip correcting angle of attack measurement system when exposed to a large sting whip error. The angle of attack ranged from -4 degrees to 10 degrees in 2 degree increments and the Mach numbers tested were from 0 to 0.9. As a

3

result of the sting whip correcting system, 85% to 90% of the error was removed and all but the extreme cases were brought within the targeted 0.01 degree angle of attack accuracy. [2]

Another transonic wind tunnel test conducted by Weiss measured model vibrations and inertial bias. Accelerations and balance readings were taken during a pitch polar at Mach 0.7 to 0.9 of a Bombardier high-speed model in the North American Trisonic Tunnel. A tri-axial accelerometer was mounted close to the model's center of gravity to measure the normal, side, and axial acceleration. A six-component internal balance was mounted on a straight sting. A qualitative analysis of the sting whip effect was completed by determining the magnitude-squared coherence function of the axial acceleration as well as the squared tangential velocity in pitch and yaw. An important conclusion from this work is that there is a link between model dynamics and inertial bias that cannot be ignored. Particularly, model dynamics can give rise to rigid body oscillations with respect to the support system. These model dynamics are distinguished by different vibration modes in normal, side, and axial directions. [4]

The specific research objectives of this thesis are to construct a state space model to represent the motion of a sting-mounted wind tunnel model, collect data from onboard accelerometers and internal balance for a variety of angles of attack and dynamic pressures that will provide good model dynamics, and apply and tune a Kalman filter to project the filtered wind tunnel measurements onto the state estimates. The ultimate goal is to demonstrate successful use of the Kalman filter technique in test article state estimation so that future wind tunnel test events can follow this approach and improve

efficiency and data accuracy. Future tests will only need to change parameter values and

perform the system identification tests to construct the stiffness matrix in order to use the

filtering technique.

CHAPTER II

KALMAN FILTER APPLICATION

In order to accomplish load and attitude estimation, a comprehensive

understanding of the Kalman filter and its application is required. This chapter will

define the Kalman filter, establish important equations, and explain how the filter will be

implemented in this research. A Kalman filter combines measurement feedback with

linear model dynamics to achieve a better state estimate than either approach alone.

Doing so removes noise from the data and projects the measurements onto the state

estimate. Measurement feedback enables effective use of instantaneous load and attitude

data rather than time-averaged data. A Kalman filter is an optimal recursive estimator

meaning the current state depends on the previous state [1]. The approach uses the

system dynamics, measurements, system noises, measurement errors, uncertainties, and

state initial conditions to estimate the current value of the state variables with a

minimized error. The state of the system is the instantaneous position, velocity, forces

and/or moments that the filter is attempting to estimate. The Kalman filter minimizes the

mean square error of the estimated state relative to the true state if all noise is Gaussian.

[5]

The main steps of the filter are state prediction, gain calculation, and state

estimate correction. The state of the system is what the filter is attempting to estimate

such as position or forces. The inputs are the measurement vector, y, and the control

input vector, u. For this work, accelerometer signals and internal balance readings are

the measurement inputs to the filter, y. The control input is the commanded angle of

attack, $u = \cos\theta_0$. The output of the filter is the state vector estimate, x which includes

aerodynamic loads, pitch and plunge values, and pitch and plunge rates. The state vector

has two values at the same time: an *a priori* estimate which is the predicted value before

the correction using the Kalman gain and an *a posteriori* estimate which is the value

after the corrections.

The Kalman filter approach outlined below is from Crassidis and Junkins [1].

This study uses the continuous-time Kalman filter since the time between samples is

sufficiently small for time to be continuous. [1]

$$\dot{x} = Ax + Bu + Gw$$

$$\hat{y} = Cx + Du + v$$

In the above equations, bold formatting signifies a vector. A is the linear state

transition model, i.e. linearized homogeneous equations of motion, and B is the control

input model. No "control" is used in this work. Instead, Bu contains the inhomogeneous

gravity load. C and D linearly transform the state vector and the control input vector,

respectively, into the expected measurements, $\hat{y}$. P is the covariance of the state vector

estimate. Covariance is the measure of how adjustments to one state are correlated with

changes in another variable. R is the estimated measurement error covariance which has

the standard deviation of the sensor noise, v, squared as the diagonal. Q is the covariance

of the process noise, w. G is the gain matrix that controls how the system noise affects

the system state and the vector w is the system noise vector. The vector v is the

measurement noise vector. The system noise vector and measurement noise vector are

not known but are characterized by Q and R respectively. $\tilde{y}$ is the vector of measurements and $\hat{y}$ is the predicted measurement value associated with states estimated by the model.

The covariance, P, is calculated by solving the continuous Riccati equation shown in Table 1. Since A, C, R, and Q are constant, $\dot{P}$ is zero. Steady state values are used for P and K. The steady state P value is calculated by setting the left-hand side of the Riccati equation equal to 0. In Matlab, this is accomplished using the continuous-time algebraic Riccati equation solution function with inputs A, C, Q, and R. The steady state value for K is calculated using the Gain equation from Table 1. Main Kalman filter equations are shown in Table 1.

Table 1. Kalman Filter Equations

Model	$\dot{x} = Ax(t) + Bu + Gw$ $\hat{y} = Cx + Du + v$
Gain	$K = PC^T R^{-1}$
Covariance	$\dot{P} = AP + PA^T - PC^T R^{-1} CP + GQG^T = 0$
Estimate	$\dot{\hat{x}} = A\hat{x} + Bu + K[\tilde{y}(t) - \hat{y}(t)]$

The term "Gw" from the model equation and the term "v" from the $\hat{y}$ equation is not included in the implementation of the Kalman filter. These values are not included because the vectors, w and v, fluctuate about zero and have the effect of increasing uncertainty, as already quantified in the P vector. In Table 1, x and y change based on time step and the rest of the terms are constant with each time step.

8

Using the equations of motion, A and B alone, it is possible to predict future system states. Of course, as time proceeds, these predictions become less accurate. To account for this, sensor measurements, $\tilde{y}$, are compared to measurements that result from the predicted states, $\hat{y}$. When the difference, the 'residual,' is non-zero, a correction can be applied to improve the estimated state accuracy. To apply the Kalman filter, first the steady-state values of the covariance of the state vector estimate, P, and the Kalman gain, K, are calculated. For the first state vector prediction, a vector of zeros is assumed as the initial condition for the estimation equation. Then, the estimation equation in Table 1 is integrated to get the corrected state vector estimate. In the correction step, the term $K[\tilde{y}-\hat{y}]$ accounts for inaccuracies in the state transition model and the random noise by the Kalman gain weighting the residual between the measurement and prediction. The goal is to minimize this residual. For each time step, the estimation equation is integrated using the corrected state vector estimate from the previous time step as the initial condition.

To help with Kalman filter performance, the Kalman gain can be tuned. A low gain weighs the model predictions more so that the filter follows the model more closely than sensor data. A high gain weighs the most recent measurement more. To adjust the Kalman gain, the process noise covariance can be adjusted since it is initially estimated. The measurement noise covariance is not adjusted since the measurement error can be estimated using knowledge of the sensors and instruments. Using these tuning properties, the filter can converge quicker and be more representative of the true state of the test article.

One problem with the experiment is the lack of knowledge of the process noise. The process noise encompasses the random forces acting on the physical system such as turbulence or varying flow conditions in the wind tunnel. Since the process noise cannot be effectively measured in this test case, it is estimated and tuned during data processing with the Kalman filter. A solution to this problem later would be to use the Autocovariance Least-Squares (ALS) Technique which estimates noise covariances from data [6]. This technique could be attempted in future work, but is not implemented here.

CHAPTER III

METHODS AND EXPERIMENTS

With the requirements and equations of the Kalman filter have been defined, the

present experiment can be introduced. The state space model based on this experiment's

test article and the wind tunnel measurements are fundamental inputs to the Kalman

filter. The experimental rig design and sensor information are explained in the following

sections.

3.1   Experimental Setup

A 1:16 scale modified WB-57 was tested at the LSWT located at Texas A&M

University. The LSWT has a 7-ft-tall by 10-ft-wide by 12-ft-long test section. The model

was built for a previous test with NASA. The model has a wingspan of 88.1 inches, an

aspect ratio of 7.5, and wing area of 1039 in^2. The model's span efficiency factor, e, is

assumed to be 0.85. This test article was chosen due to the dynamic motion observed

during a previous experiment. An internal balance was mounted onto the LSWT High

Attitude Robotic Sting (HARS) system. The HARS system controls the pitch and roll of

the model while keeping the model centered in the test section. The sting and balance

system was then internally secured to the model using a balance block. Figure 1 shows

the sting and balance system installed in the wind tunnel test section.
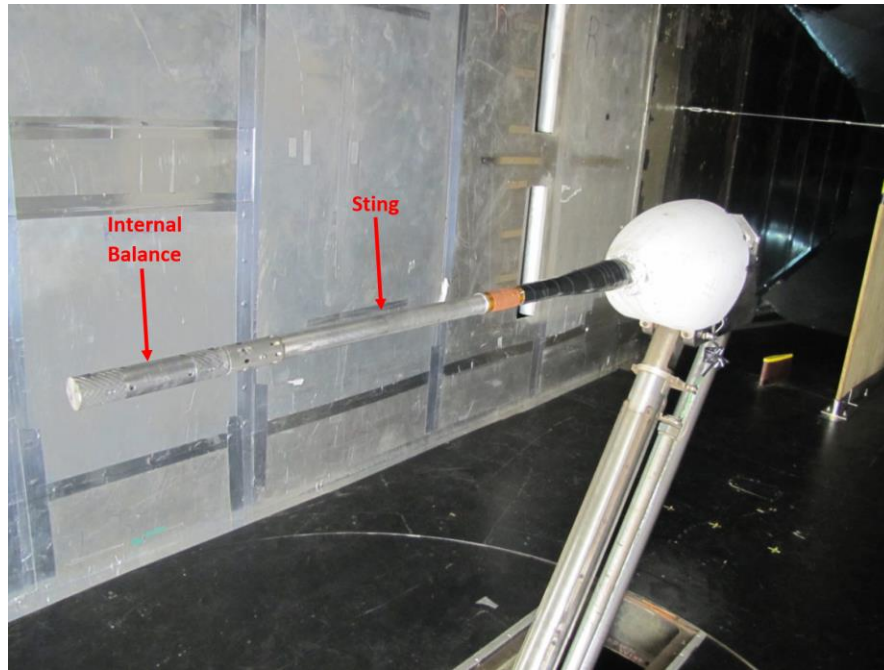
Figure 1. Sting and Balance Installation in the Wind Tunnel Test Section.

The internal balance measures the aerodynamic forces and moments. Internal balance limits are discussed in the next section. Single-axis accelerometers were mounted on the inside and outside of the model. Two accelerometers were mounted along the centerline inside the model, one accelerometer was mounted externally on the port wing, and the last was mounted on the starboard wing. The offset of the two centerline accelerometers allowed for the pitch or plunge angle to be calculated. In the Accelerometers section, the specifications and locations of the accelerometers are tabulated and labeled. The complete experimental set up with the model mounted onto the sting is shown in Figure 2. Flow is from the left to right.
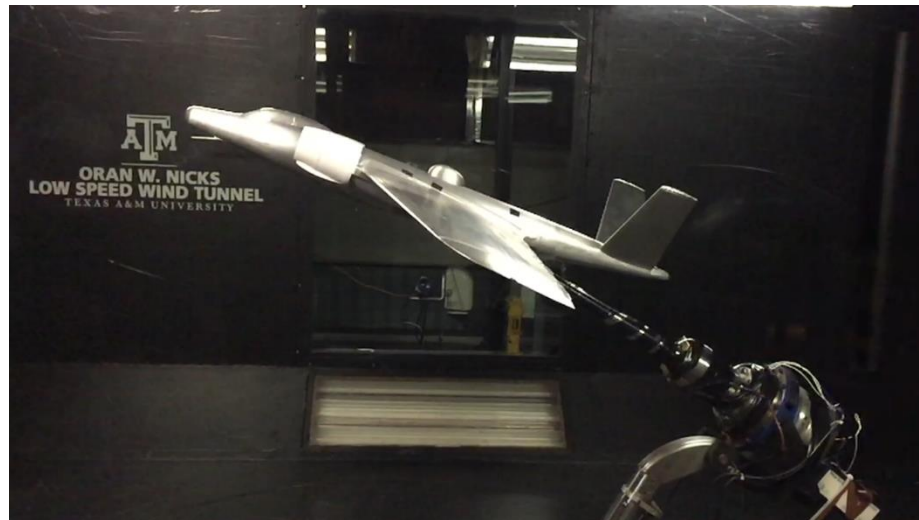
Figure 2. WB-57 Modified Model Installed in the LSWT Test Section.

The internal balance used in the experiment is the Task Corporation Mark XIII. The Mark XIII is a strain gauge internal balance that measures two normal force loads, two side force loads, an axial force load, and a rolling moment. Pitch and yaw moments are calculated from the respective forces and known distances between the gauges. The limits of the balance are displayed in Table 2. Figure 3 shows a close-up view of the Mark XIII internal balance that is mounted inside of the test article. The diameter of the internal balance is 1.25 inch.

Table 2. Mark XIII Internal Balance Limits

Mark XIII Internal Balance Limits	
N1, N2	500 lb$_f$, ±0.4 lb$_f$
S1, S2	500 lb$_f$, ±0.5 lb$_f$
Axial Force	150 lb$_f$, ±0.1 lb$_f$
Rolling Moment	800 in.lb$_f$, ±1.7 in.lb$_f$
Pitching Moment	2625 in.lb$_f$
Yawing Moment	2125 in.lb$_f$

Figure 3. Close-up View of the Mark XIII Internal Balance.

All accelerometers were purchased from PCB Piezotronics. Specific information about each accelerometer is shown in Table 3 and the physical location of each accelerometer is shown in Figure 4.

Table 3. Accelerometer Specifications and Physical Location of Sensor Mounting.

	Location of Accelerometer	Model Number	Serial Number	Sensitivity (mV/g)	Bias Level (V)
1	Center Front	352C68	122350	98.8 (10.07 mV/m/s^2)	11.3
2	Center Rear	352C68	124921	98.2 (10.02 mV/m/s^2)	11.1
3	Port Wing	333B40	40733	498 mV/g (50.7 mV/m/s^2)	10.9
4	Starboard Wing	333B40	47712	490 mV/g (49.9 mV/m/s^2)	11.1
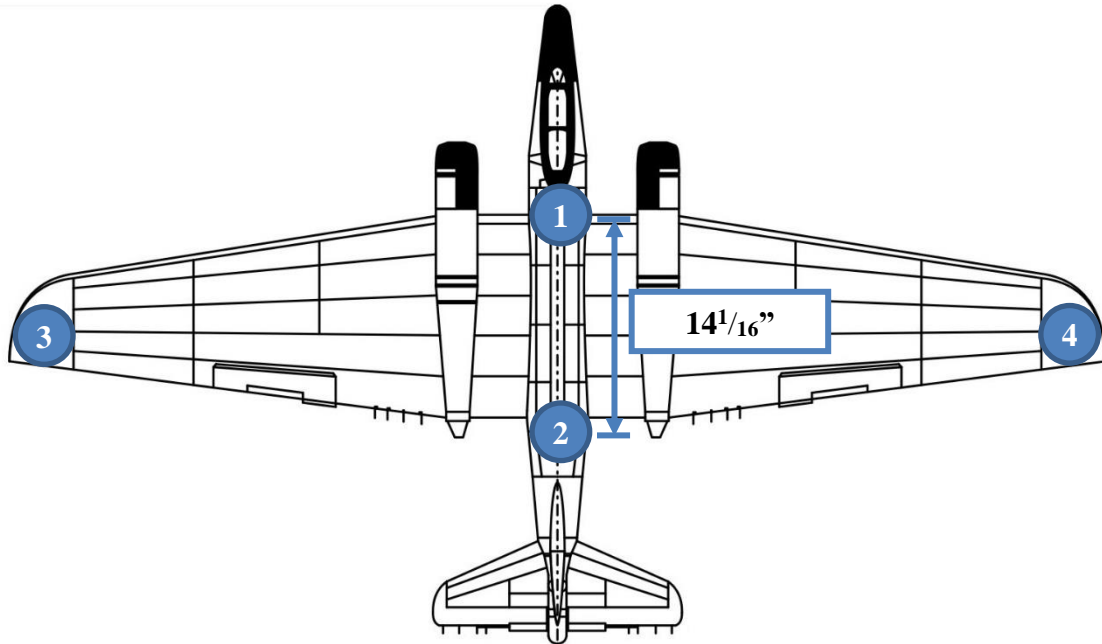
Figure 4. Visual Location of Accelerometers on WB-57 Planform. [7]

3.2   Experiments

Table 4 is the test matrix for the wind tunnel testing. Data was collected on 5 April 2017 at the LSWT. Each data point includes 20,000 samples collected at 1 kHz. Prior to wind-on testing, rap tests (that is, striking the test article with a mallet) were completed to determine the weight and natural frequencies of the model and aid in constructing the A and C matrices for the Kalman filter. For this test, the roll angle is 0° and the angle of attack is commanded to a value determined by the test point configuration.

The first set of data points are the conventional sting deflections where weight is added to the model with wind-off and the commanded pitch angle set to 0. Rap tests are then completed with wind-off. During the rap tests, a mallet strikes the test article to get the ring-down characteristics for system identification. The location of the mallet strike depends on which system response is being identified. For pitch, the mallet strikes three locations on the model: the nose, center of the model, and the tail. The last wind-off test is the conventional static tare pitch sweep from -10° to 20°. These data points are used in the traditional data reduction where the static tare is removed from the internal balance sensors to get the aerodynamic loads. However, the static tare data is not removed from the single α runs to get the aerodynamic loads. Instead, the aerodynamic load is a state for estimation and the internal balance reading is a traditional measurement. Single α runs are completed at each commanded pitch angle and dynamic pressure with internal balance and accelerometer data collected. The pitch angle range is from -10° to 20° with 2° intervals. The dynamic pressures tested are 7.5 psf, 15 psf, and 22.5 psf.

16

Table 4. Test Matrix

Run Number	Configuration	Test Name	Commanded Pitch Angle
13	Wind-off	Conventional Sting Deflection	0
13	Wind-off	Pitch Rap Tests (Nose, Center, Tail)	0
13	Wind-off	Roll Rap Tests (Port Wing Tip, Center, Starboard Wing Tip)	0
13	Wind-off	Yaw Rap Tests (Port Side of Nose, Trailing Edge of Port Wing, Starboard Side of Tail)	0
14	Wind-off	Static Tare	-10° to 20° by 2°
15	Wind-on q=7.5 psf	Single α Runs	-10° to 20° by 2°
16	Wind-on q=15 psf	Single α Runs	-10° to 20° by 2°
17	Wind-on q=22.5 psf	Single α Runs	-10° to 20° by 2°

CHAPTER IV

GOVERNING EQUATIONS AND STATE-SPACE MODEL

In order to use a Kalman filter, a linearized state space model is required. The derivation of the governing equations is discussed below. The complete state space model is summarized at the end of this chapter. Important quantities used in the derived equations and in the free body diagrams of Figure 5 and Figure 6 are defined above in the Nomenclature section.

Figure 5 and Figure 6 show annotated free body diagrams of the model and sting/internal balance systems respectively. Equations are derived in the conventional aircraft body-fixed frame. The +x direction is pointed out the aircraft's nose. The +z direction is pointed downward and the +y direction is pointed out the starboard wing. Positive theta is rotation about the +y axis.
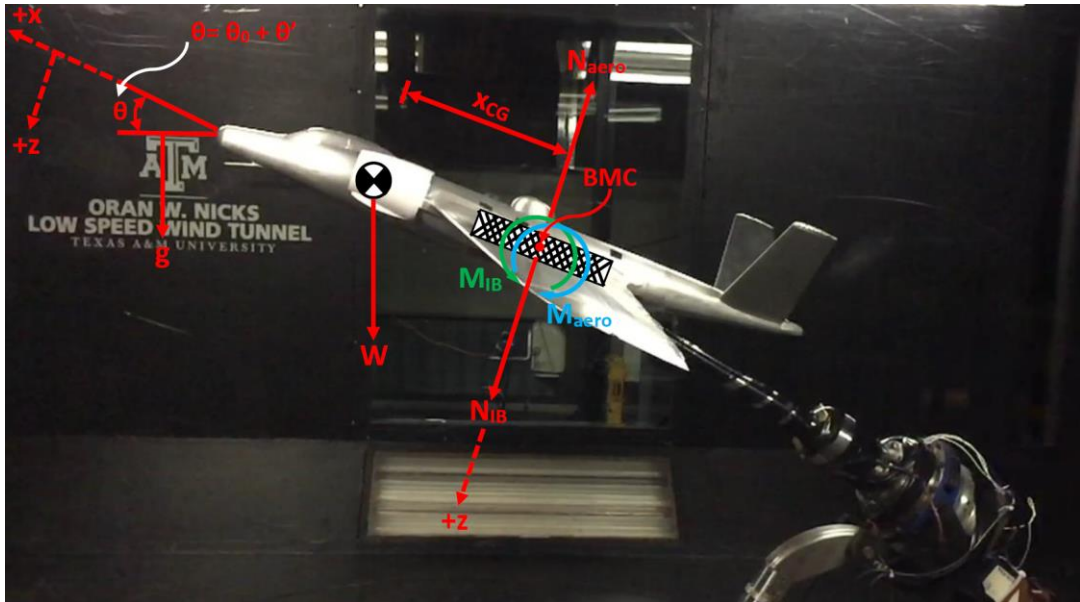
Figure 5. Free Body Diagram of Model Shown Installed in the LSWT Test Section.
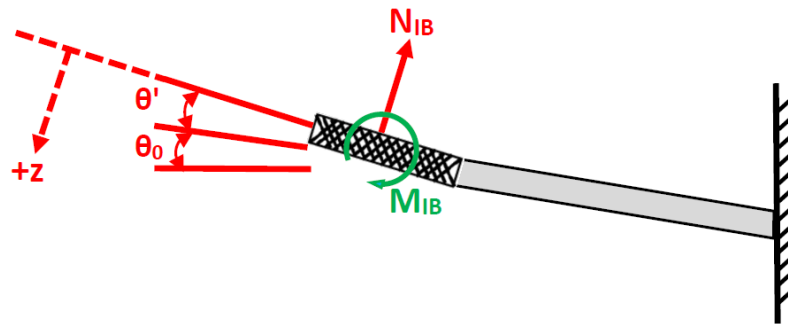
Figure 6. Free Body Diagram of the Sting/Internal Balance.

The derivation of the equations of motion begin with summing all forces and moments acting on the test article in the body-fixed frame. The forces acting on the test article in the z-direction are the normal force due to aerodynamic forces, the normal

force applied to the model by the sting through the internal balance, and the weight. The

moments acting on the test article are the aerodynamic pitching moment about the

balance moment center (BMC), the pitching moment applied through the internal

balance, and the moment due to the weight acting at the center of the gravity.

Conservation of z-momentum

$$N_{IB} - N_{aero} + W\cos(\theta_0 + \theta') = \frac{W}{g}\ddot{z}'$$

$$\ddot{z}' = \frac{g}{W}N_{IB} - \frac{g}{W}N_{aero} + g\cos(\theta_0 + \theta')$$

Conservation of y-angular momentum

$$r_{g,yy}^2 = \frac{I_{yy}}{m}$$

$$-M_{IB} + M_{aero,BMC} - W\cos(\theta_0 + \theta')\,x_{CG} = \frac{W}{g}r_g^2\ddot{\theta}'$$

$$\ddot{\theta}' = -\frac{g}{Wr_g^2}M_{IB} + \frac{g}{Wr_g^2}M_{aero,BMC} - \frac{g}{r_g^2}\cos(\theta_0 + \theta')\,x_{CG}$$

For this study, θ' is considered a small angle and a small angle approximation is

used. Therefore, cos(θ')≈1 and sin(θ')≈θ'. Also, (θ')²≈0. Using this approximation, the

above equations for $\ddot{z}'$ and are $\ddot{\theta}'$ simplified to:

$$\ddot{z}' = \frac{g}{W}N_{IB} - \frac{g}{W}N_{aero} + g\cos\theta_0 - g\theta'\sin\theta_0 \qquad (1)$$

$$\ddot{\theta}' = -\frac{g}{Wr_g^2}M_{IB} + \frac{g}{Wr_g^2}M_{aero,BMC} - \frac{gx_{CG}}{r_g^2}\cos\theta_0 + \frac{gx_{CG}}{r_g^2}\theta'\sin\theta_0 \qquad (2)$$

The internal balance attached to the sting acts as a cantilevered beam with a force

or moment applied at the end. Using beam deflection equations for a load and moment

applied separately at the end of the beam, equations for the normal force due to the internal balance and the internal balance pitching moment can be derived.

Load Applied at End of Beam

$$z' = -\frac{N_{IB}L^3}{3EI}$$

$$\theta' = \frac{N_{IB}L^2}{2EI}$$

Moment Applied at End of Beam

$$z' = -\frac{M_{IB}L^2}{2EI}$$

$$\theta' = \frac{M_{IB}L}{EI}$$

Rearranging to Calculate Stiffness Matrix

$$\begin{bmatrix} z' \\ \theta' \end{bmatrix} = \begin{bmatrix} -L^3/3EI & -L^2/2EI \\ L^2/2EI & L/EI \end{bmatrix} \begin{bmatrix} N_{IB} \\ M_{IB} \end{bmatrix}$$

$$\begin{bmatrix} N_{IB} \\ M_{IB} \end{bmatrix} = \begin{bmatrix} -12EI/L^3 & -6EI/L^2 \\ 6EI/L^2 & 4EI/L \end{bmatrix} \begin{bmatrix} z' \\ \theta' \end{bmatrix}$$

$$\begin{bmatrix} N_{IB} \\ M_{IB} \end{bmatrix} = \underbrace{\begin{bmatrix} k_{NZ} & k_{N\theta} \\ k_{MZ} & k_{M\theta} \end{bmatrix}}_{} \begin{bmatrix} z' \\ \theta' \end{bmatrix}$$

Stiffness Matrix, k

$$N_{IB} = k_{NZ}z' + k_{N\theta}\theta' \tag{3}$$

$$M_{IB} = k_{MZ}z' + k_{M\theta}\theta' \tag{4}$$

In reality, the stiffness matrix comes from data collected during the wind tunnel test from the wind-off system identification tests. The system identification tests determine the weight and natural frequencies of the model and in turn the stiffness matrix from k=w_n^2m. The stiffness matrix given above is estimated using estimated values for L, E, and I. L is the sting length, E is the elastic modulus, and I is the area moment of inertia of the sting. The true stiffness values come from the system identification tests and are used in the Kalman filter state-space equations.

Substituting the Equations (3) and (4) for beam bending into Equations (1) and (2) gives Equations (5) and (6) respectively. Equations 5 and 6 are the main motion equations that are used in the state space model.

$$\ddot{z}' = \left({k_{NZ}g}/{W}\right)z' + \left({k_{N\theta}g}/{W}\right)\theta' - \frac{g}{W}N_{aero} + g\cos\theta_0 - g\theta'\sin\theta_0 \qquad (5)$$

$$\ddot{\theta}' = -\left({k_{MZ}g}/{Wr_g^2}\right)z' - \left({k_{M\theta}g}/{Wr_g^2}\right)\theta' + \frac{g}{Wr_g^2}M_{aero,BMC} - \frac{gx_{CG}}{r_g^2}\cos\theta_0$$

$$+ \frac{gx_{CG}}{r_g^2}\theta'\sin\theta_0 \qquad (6)$$

Even though the model is dynamic, steady aerodynamics are assumed to simplify the above equations. The linear region of the lift curve is assumed and the lift curve slope is approximated as a≈2π. Furthermore, it is assumed that α_0 and θ' are small. In an actual wind tunnel test, the lift is not zero at 0° angle of attack ($\alpha_0 \neq 0°$) because of blockage corrections and the lift curve slope is not equal to 2π due to the finite wing. However, the state transition model does not need to be exact, only reasonably good so that the Kalman filter can converge quickly to estimate the states. Therefore, these approximations are expected to be sufficient. A drag approximation is included in the

normal force. Since the order of magnitude of drag is less than the order of magnitude of lift, there would be a minimal effect on the results if the drag approximation diverges from the exact value.

The angle of attack, α, is approximately equal to θ which is the sum of the commanded angle of attack, $θ_0$, and the rotation from the commanded angle of attack due to unsteadiness of model, θ'. The derivative of θ with respect to time is $\dot{θ}'$ since $θ_0$ is constant. The derivation of the aerodynamic normal force is shown below by applying the above assumptions to the lift and drag coefficients, calculating the lift and drag forces, and then resolving the lift and drag forces into the normal force, N_{aero}.

$$C_L = a(\alpha - \alpha_0) \qquad where\ a = \frac{dC_L}{d\alpha} \approx 2\pi$$

$$L = a(\alpha - a_0)qS \approx a\alpha qS$$

$$C_D = C_{D,0} + \frac{C_L^2}{\pi eAR}$$

$$D = \left(C_{D,0} + \frac{C_L^2}{\pi eAR}\right)qS \approx \left(C_{D,0} + \frac{a^2\alpha^2}{\pi eAR}\right)qS$$

$$N_{aero} = L\cos\alpha + D\sin\alpha$$

$$N_{aero} \approx aqS\alpha\cos\alpha + \left(C_{D,0} + \frac{a^2\alpha^2}{\pi eAR}\right)qS\sin\alpha$$

$$N_{aero} \approx qS\left(a\alpha\cos\alpha + C_{D,0}\sin\alpha + \frac{a^2\alpha^2}{\pi eAR}\sin\alpha\right)$$

Substitute $θ_0 + θ'$ for α:

$$N_{aero} \approx qS\left(a(\theta_0 + \theta')\cos(\theta_0 + \theta') + C_{D,0}\sin(\theta_0 + \theta')\right.$$

$$\left. + \frac{a^2(\theta_0 + \theta')^2}{\pi e AR}\sin(\theta_0 + \theta')\right)$$

Expanding $\sin(\theta)$ and $\cos(\theta)$ and simplifying using the small angle assumption for θ' as well as assuming that $(\theta')^2$ and $\theta'\sin(\theta_0)$ are very small (≈ 0):

$$N_{aero} \approx qS\left(a\theta_0\cos\theta_0 + a\theta'\cos\theta_0 + C_{D,0}\sin\theta_0 + C_{D,0}\theta'\cos\theta_0\right.$$

$$\left. + \frac{a^2}{\pi e AR}(\theta_0^2\sin\theta_0 + \theta_0^2\theta'\cos\theta_0)\right) \tag{7}$$

$$\frac{dN}{dt} = \dot{N}_{aero} = qS\left(a\cos\theta_0 + C_{D,0}\cos\theta_0 + \frac{a^2}{\pi e AR}\theta_0^2\cos\theta_0\right)\dot{\theta}' \tag{8}$$

The aerodynamic axial force derivation is shown below. However, the aerodynamic axial force is only a function of θ_0, therefore, the time derivative of A_{aero} is 0 since θ_0 is constant over time. The axial force will not be included in the state space model. From the assumptions and calculations previously shown in the aerodynamic normal force derivation, the lift and drag equations are:

$$L \approx a\alpha qS$$

$$D \approx \left(C_{D,0} + \frac{a^2\alpha^2}{\pi e AR}\right)qS$$

Resolving the lift and drag forces into the aerodynamic axial force gives:

$$A_{aero} = -L\sin\alpha + D\cos\alpha$$

$$A_{aero} = -a\alpha qS\sin\alpha + \left(C_{D,0} + \frac{a^2\alpha^2}{\pi e AR}\right)qS\cos\alpha$$

Substitute $\theta_0 + \theta'$ for α:

$$A_{aero} = -a(\theta_0 + \theta')qS\sin(\theta_0 + \theta') + \left(C_{D,0} + \frac{a^2(\theta_0 + \theta')^2}{\pi eAR}\right)qS\cos(\theta_0 + \theta')$$

Expanding $\sin(\theta)$ and $\cos(\theta)$ and simplifying using the small angle assumption

for θ' as well as assuming that $(\theta')^2$ and $\theta'\sin(\theta_0)$ and $\theta'\theta_0$ are very small (≈ 0):

$$A_{aero} = qS\left(-a\theta_0\sin\theta_0 + C_{D,0}\cos\theta_0 + \frac{a^2}{\pi eAR}\theta_0{}^2\cos\theta_0\right) = f(\theta_0)$$

$$\frac{dA_{aero}}{dt} = 0$$

The next important derivation for the state space model is the aerodynamic

pitching moment about the BMC. The aerodynamic pitching moment about the BMC is

the sum of the moment caused by the normal force and the aerodynamic pitching

moment about the aerodynamic center. In the absence of knowledge of the true

aerodynamic center, the location of the aerodynamic center is taken to be at the quarter

chord location of the wing.

$$M_{BMC} = \underbrace{N_{aero}x_{AC} + M_{aero,AC}}_{M_{aero,BMC}} - Wx_{CG}\cos\theta$$

$$M_{aero,BMC} = N_{aero}x_{AC} + M_{aero,AC}$$

Taking the derivative of the aerodynamic pitching moment about the BMC with

respect to time gives:

$$\frac{dM_{aero,BMC}}{dt} = \frac{dN_{aero}}{d\alpha}\frac{d\alpha}{dt}x_{AC} + \frac{dM_{aero,AC}}{d\alpha}\frac{d\alpha}{dt}$$

The time derivative of the angle of attack is approximately equal to the time

derivative of the rotation from the commanded angle of attack, θ'. The derivative of the

aerodynamic pitching moment about the aerodynamic center with respect to the angle of

attack is approximately 0. These two approximations simplify the equation for the time

derivative of the aerodynamic pitching moment about the BMC.

$$\frac{d\alpha}{dt} = \frac{d\theta'}{dt} \quad and \quad \frac{dM_{aero,AC}}{d\alpha} \approx 0$$

$$\frac{dM_{aero,BMC}}{dt} = \frac{dN_{aero}}{d\alpha} \frac{d\theta'}{dt} x_{AC}$$

In order to get the full equation for the time derivative of $M_{aero,BMC}$, the derivative

of the aerodynamic normal with respect to angle of attack needs to be computed. This is

shown below.

$$N_{aero} \approx qS\left(a\alpha \cos\alpha + C_{D,0}\sin\alpha + \frac{a^2\alpha^2}{\pi e AR}\sin\alpha\right)$$

$$\frac{dN_{aero}}{d\alpha} = qS\left(-a\alpha\sin\alpha + a\cos\alpha + C_{D,0}\cos\alpha + \frac{a^2\alpha^2}{\pi e AR}\cos\alpha + \frac{2a^2\alpha}{\pi e AR}\sin\alpha\right)$$

Replacing α with $\theta=\theta_0+\theta$':

$$\frac{dN_{aero}}{d\alpha} = qS\left(-a(\theta_0 + \theta')\sin(\theta_0 + \theta') + a\cos(\theta_0 + \theta') + C_{D,0}\cos(\theta_0 + \theta')\right.$$

$$\left. + \frac{a^2(\theta_0 + \theta')^2}{\pi e AR}\cos(\theta_0 + \theta') + \frac{2a^2(\theta_0 + \theta')}{\pi e AR}\sin(\theta_0 + \theta')\right)$$

Expanding $\sin(\theta)$ and $\cos(\theta)$ and simplifying using the small angle assumption

for θ':

$$\frac{dN_{aero}}{d\alpha} = qS\left(-a\theta_0 \sin\theta_0 + a\theta_0\theta' \cos\theta_0 + a\theta' \sin\theta_0 + a(\theta')^2 \cos\theta_0 + a\cos\theta_0\right.$$

$$- a\theta' \sin\theta_0 + C_{D,0} \cos\theta_0 - C_{D,0}\theta' \sin\theta_0 + \frac{a^2}{\pi eAR}\theta_0{}^2 \cos\theta_0$$

$$+ \frac{2a^2}{\pi eAR}\theta_0\theta' \cos\theta_0 - \frac{a^2\theta_0^2}{\pi eAR}\theta' \sin\theta_0 - \frac{2a^2}{\pi eAR}\theta_0(\theta')^2 \sin\theta_0$$

$$+ \frac{2a^2}{\pi eAR}\theta_0 \sin\theta_0 + \frac{2a^2}{\pi eAR}\theta' \sin\theta_0 + \frac{2a^2}{\pi eAR}\theta_0\theta' \cos\theta_0$$

$$\left. + \frac{2a^2}{\pi eAR}(\theta')^2 \cos\theta_0\right)$$

Assuming that $(\theta')^2$ and $\theta'\sin(\theta_0)$ are very small (≈ 0) and that $\theta'\theta_0$ is relatively small (≈ 0) since the value of θ_0 between 0° and 20°, the equation simplifies to:

$$\frac{dN}{d\alpha} = qS\left(-a\theta_0 \sin\theta_0 + a\cos\theta_0 + C_{D,0} \cos\theta_0 + \frac{a^2}{\pi eAR}\theta_0{}^2 \cos\theta_0\right.$$

$$\left. + \frac{2a^2}{\pi eAR}\theta_0 \sin\theta_0\right) \tag{9}$$

$$\frac{dM_{aero,BMC}}{dt} = qSx_{AC}\left(-a\theta_0 \sin\theta_0 + a\cos\theta_0 + C_{D,0} \cos\theta_0 + \frac{a^2}{\pi eAR}\theta_0{}^2 \cos\theta_0\right.$$

$$\left. + \frac{2a^2}{\pi eAR}\theta_0 \sin\theta_0\right)\dot\theta' \tag{10}$$

The state space model for the Kalman filter uses Equations 5, 6, 8, and 10. All assumptions and estimates presented in this study are to construct a reasonably good model where the Kalman filter will account for the model imperfections. The Kalman filter accounts for the imperfections by multiplying the difference between the true measurements and predicted measurements by the Kalman gain. The more accurate the

model, the more quickly the filter is expected to converge. The only control input in this study is the commanded angle of attack. Therefore, the u vector only includes a variable in u_1.

$$u_1 = \cos\theta_0$$

$$x_1 = z'$$

$$x_2 = \dot{z}' = \dot{x}_1$$

$$x_3 = N_{aero}$$

$$x_4 = \theta'$$

$$x_5 = \dot{\theta}' = \dot{x}_4$$

$$x_6 = M_{aero,BMC}$$

$$\dot{x}_1 = \dot{z}' = x_2$$

$$\dot{x}_2 = \ddot{z}' = \left(\frac{k_{NZ}g}{W}\right)x_1 + \left(\frac{k_{N\theta}g}{W}\right)x_4 - \frac{g}{W}x_3 - g\sin\theta_0\,x_4 + gu_1$$

$$\dot{x}_3 = \frac{dN_{aero}}{dt} = qS\left(a\cos\theta_0 + C_{D,0}\cos\theta_0 + \frac{a^2}{\pi eAR}\theta_0^2\cos\theta_0\right)x_5$$

$$\dot{x}_4 = \dot{\theta}' = x_5$$

$$\dot{x}_5 = \ddot{\theta}' = -\left(\frac{k_{MZ}g}{Wr_g^2}\right)x_1 - \left(\frac{k_{M\theta}g}{Wr_g^2}\right)x_4 + \frac{g}{Wr_g^2}x_6 + \frac{gx_{CG}}{r_g^2}\sin\theta_0\,x_4$$

$$-\frac{gx_{CG}}{r_g^2}u_1$$

$$\dot{x}_6 = \frac{dM_{aero,BMC}}{dt}$$

$$= qSx_{AC}\left(-a\theta_0\sin\theta_0 + a\cos\theta_0 + C_{D,0}\cos\theta_0 + \frac{a^2}{\pi eAR}\theta_0{}^2\cos\theta_0\right)$$

$$+ \frac{2a^2}{\pi eAR}\theta_0\sin\theta_0\Bigg)x_5$$

Putting the above equations in matrix form which is necessary for Kalman filter application:

$$\dot{\boldsymbol{x}} = A\boldsymbol{x} + B\boldsymbol{u} + G\boldsymbol{w}$$

$$\hat{\boldsymbol{y}} = C\boldsymbol{x} + D\boldsymbol{u} + \boldsymbol{v}$$

A is a 6x6 matrix. B and x are 6x1 vectors and u is a 1x1 vector. C is a 4x6 matrix and D is 4x1 vector.

Non-zero components of A matrix:

$$A_{1,2} = 1$$

$$A_{2,1} = \frac{k_{NZ}g}{W}$$

$$A_{2,3} = -\frac{g}{W}$$

$$A_{2,4} = \frac{k_{N\theta}g}{W} - g\sin\theta_0$$

$$A_{3,5} = qS\left(a\cos\theta_0 + C_{D,0}\cos\theta_0 + \frac{a^2}{\pi eAR}\theta_0{}^2\cos\theta_0\right)$$

$$A_{4,5} = 1$$

$$A_{5,1} = -\frac{k_{MZ}g}{Wr_g^2}$$

$$A_{5,4} = -\frac{k_{M\theta}g}{Wr_g^2} + \frac{gx_{CG}\sin\theta_0}{r_g^2}$$

$$A_{5,6} = \frac{g}{Wr_g^2}$$

$$A_{6,5} = qSx_{AC}\left(-a\theta_0\sin\theta_0 + a\cos\theta_0 + C_{D,0}\cos\theta_0 + \frac{a^2}{\pi eAR}\theta_0{}^2\cos\theta_0\right.$$

$$\left. + \frac{2a^2}{\pi eAR}\theta_0\sin\theta_0\right)$$

Non-zero components of B matrix:

$$B_{2,1} = g$$

$$B_{5,1} = -\frac{gx_{CG}}{r_g^2}$$

Non-zero components of C matrix:

$$C_{1,1} = \frac{k_{NZ}g}{W}$$

$$C_{1,3} = \frac{-g}{W}$$

$$C_{1,4} = \frac{k_{N\theta}g}{W} - g\sin\theta_0$$

$$C_{2,1} = \frac{-k_{MZ}g}{Wr_g^2}$$

$$C_{2,4} = -\frac{k_{M\theta}g}{Wr_g^2} + \frac{gx_{CG}}{r_g^2}\sin\theta_0$$

$$C_{2,6} = \frac{g}{Wr_g^2}$$

$$C_{3,1} = k_{NZ}$$

$$C_{3,4} = k_{N\theta}$$

$$C_{4,1} = k_{MZ}$$

$$C_{4,4} = k_{M\theta}$$

Non-zero components of D matrix:

$$D_{1,1} = g$$

$$D_{2,1} = \frac{g x_{CG}}{r_g^2}$$

4.1   Matlab Kalman Filter Implementation

The Kalman filter is implemented using Matlab. All constants and matrices using the above equations are defined. Data is loaded into the script for each test run and data point corresponding to Appendix A. The angle of attack and dynamic pressure are changed for each data point. A pseudocode is presented below to show the steps that were taken to get the post-Kalman filter results [8].

1. Define all constants. Define dynamic pressure and angle of attack based on data file being filtered.

2. Define state space matrices for A, B, C, D, and u.

3. Define noise covariance matrices Q and R.

4. Calculate the steady-state value for P using Matlab's continuous algebraic Riccati function.

5. Import processed data

    a. Save z acceleration, theta acceleration, N_{IB}, M_{IB} to the $x_{measured}$ matrix. If needed, convert units from English to SI units.

6. Calculate the steady-state value of the Kalman gain.

7. Set the first initial condition of the state vector estimate.

8. For each time step integrate $\dot{x} = Ax + Bu + K[y(t) - (Cx + Du)]$ using

   Matlab's ode15s with the initial condition and measurements from this time step.

9. Plot results.

CHAPTER V

ANALYSIS

Before discussing the results of the experiment and filtering technique, several

procedures are completed using the collected data that are necessary before applying the

state estimation technique. These include calculating plunge and pitch acceleration from

sensors readings, identifying specific model parameters such as weight and moment of

inertia, and calculating sensor noise.

5.1   State System Measurements

The strain gauges readings from the internal balance are converted to pounds-

force. The total normal force is calculated by adding the N1 and N2 data. The pitching

moment is calculated by subtracting the N2 reading from the N1 reading and multiplying

by the distance between the two strain gauges, 5.25 inches (0.1334 meters). The z-

acceleration is calculated by averaging the centerline accelerometers readings. The pitch

acceleration is calculated by subtracting the back centerline accelerometer from the front

centerline accelerometer and dividing by the distance between them.

5.2   System Identification Analysis

Using data from a static tare run show the model to weigh 159 lbf (708 N). The

estimated weight from the Solidworks design file is 158 lbf (705 N). The center of

gravity location was calculated using N1 and N2 internal balance strain gauge readings

during the static tare run and determining the location where these two strain gauge readings were equivalent. This yielded a center of gravity 24 inches (0.621 meters) from the nose of the aircraft model. The center of gravity location from Solidworks is 21.8 inches (0.553 meters). The pitch moment of inertia, I_{yy}, is calculated using the Equation 11 below where m is the mass of the model, g is the acceleration due to gravity, d is the distance from the axis of rotation to the center of gravity, and ω is the frequency. I_{yy} calculated from the system identification is 24.4 kg-m^2. From Solidworks, I_{yy} is 25.1 kg-m^2.

$$I_{axis} = \frac{mgd}{\omega^2} \qquad (11)$$

Overall similarity between these values and predicted values is surprisingly good. Measurement noise is quantified with the innate bias and collected data standard deviation of the internal balance strain gauges, N1 and N2, and the centerline accelerometers. The bias error is taken from the instruments specification sheets. The centerline accelerometers have a bias of 10% of the sensitivity. The sensitivities of the accelerometers are calculated by finding the voltage output during the static tare run at 0° angle of attack. The front centerline accelerometer has a bias of 0.0067 m/s^2 and the back centerline accelerometer has a bias of 0.0016 m/s^2. The two biases were squared, added, and square rooted to find the combined error, $\sigma_{bias,accel}$, which is 0.0069 m/s^2. For z-acceleration and theta-acceleration, the standard deviations of the individual accelerometers were combined similarly. The standard deviation of front centerline accelerometer is 0.15 m/s^2 and the standard deviation of the back centerline accelerometer is 0.17 m/s^2. The combined standard deviation, $\sigma_{random,z\ accel}$, of the z

34

acceleration is 0.0015 m/s². The combined standard deviation, $\sigma_{random,theta\ accel}$, of the theta acceleration is 0.0017 rad/s². The innate bias, $\sigma_{bias,N}$, of the normal force is 1.4 N. The innate bias of the pitching moment, $\sigma_{bias,PM}$, is 0.19 N-m. For the internal balance normal force and the pitching moment, the standard deviations of the N1 and N2 strain gauges were calculated and added similarly. The standard deviation of the N1 strain gauge is 3.2 N and the standard deviation of the N2 strain gauge is 3.2 N. The combined normal force standard deviation, $\sigma_{random,N}$, is 4.5 N. The combined pitching moment standard deviation, $\sigma_{random,PM}$, is 0.6 N-m. These values are included in the determination of the measurement error covariance matrix, R with the non-zero values of R shown below.

$$R_{1,1} = \sigma^2_{bias,accel} + \sigma^2_{random,accel} = (0.0069)^2 + (0.0015)^2 = 0.00005 \left(\frac{m}{s^2}\right)^2$$

$$R_{2,2} = \sigma^2_{bias,accel} + \sigma^2_{random,accel} = (0.0069)^2 + (0.0017)^2 = 0.00051 \left(\frac{rad}{s^2}\right)^2$$

$$R_{3,3} = \sigma^2_{bias,N} + \sigma^2_{random,N} = (1.4)^2 + (4.5)^2 = 22.21\ N^2$$

$$R_{4,4} = \sigma^2_{bias,PM} + \sigma^2_{random,PM} = (0.19)^2 + (0.6)^2 = 0.396\ (Nm)^2$$

5.2.1 Stiffness Matrix Extraction

The natural frequency is computed by finding the logarithmic decrement following a rap test. Plots of the rap pitch total normal force and pitching moment are evaluated to find t, T, n, x(t), and x(t+nT). Using these values, the logarithmic decrement, δ, is calculated using Equation 12. The logarithmic decrement is useful for calculating the damping ratio, ζ. The damped frequency, w_d, is calculated using the

period, T. The natural frequency, w_n, is calculated using the damped frequency and the damping ratio. The equations for damping ratio, damped frequency, and natural frequency are shown in Equations 13, 14, and 15 respectfully. An example of the one of the rap pitch tests outputs in shown in Figure 7 for an impulse at the nose of the model.

$$\delta = \frac{1}{n} \ln \left(\frac{x(t)}{x(t + nT)} \right) \tag{12}$$

$$\zeta = \frac{1}{\sqrt{1 + \left(\frac{2\pi}{\delta} \right)^2}} \tag{13}$$

$$w_d = \frac{2\pi}{T} \tag{14}$$

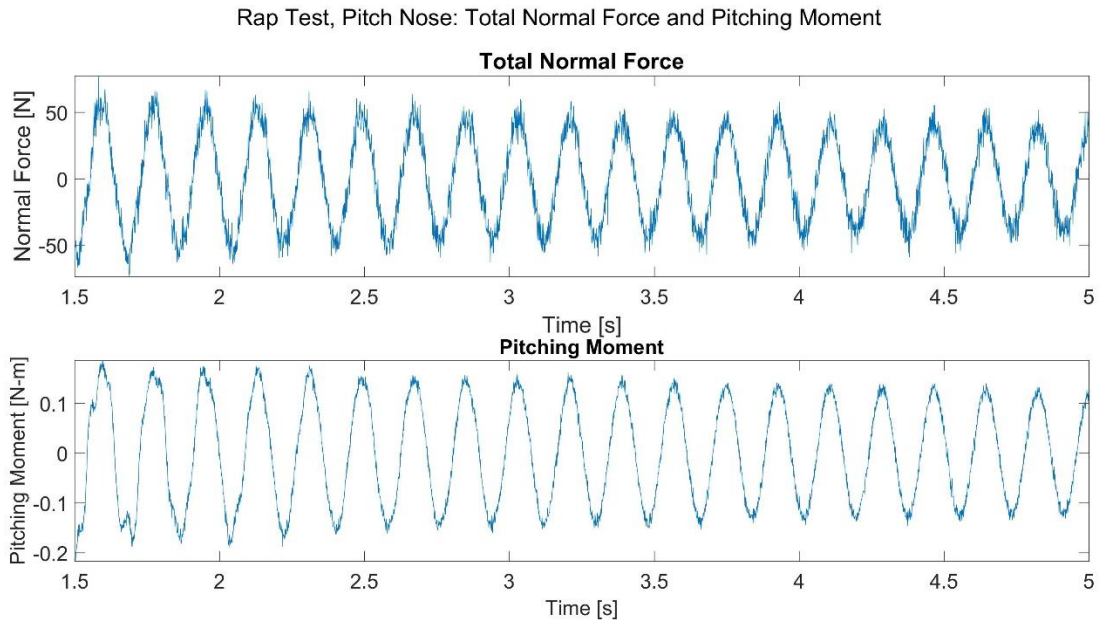$$w_n = \frac{w_d}{\sqrt{1 - \zeta^2}} \tag{15}$$

Figure 7. *Total Normal Force and Pitching Moment Responses for Rap Pitch Test with*

Impulse at the Nose.

36

Using Equation 16 for the transient response of an underdamped harmonic oscillator, the constants of the function (A, σ, ω, and φ) are calculated such that the plot directly matches the rap pitch test responses. Figure 8 shows the transient response function in red overlapping the rap pitch test in blue that is also shown in Figure 7. Appendix B shows all of the rap pitch tests with Equation 16 superposed.

$$y = Ae^{-\sigma t}\cos(\omega t + \varphi) \tag{16}$$

In Equation 16, A is a constant, σ is the exponential decay of oscillations, ω is the angular frequency, and φ is the phase. For all three of the rap pitch tests, σ and ω should be similar. The stiffness, k, is calculated using w_n^2/m and w_n is calculated from $\sqrt{\sigma^2 + \omega^2}$. Table 5 shows the value of these constants for each of the rap pitch tests for the total normal force. Table 6 shows the value of these constants for each of the rap pitch tests for the pitching moment.
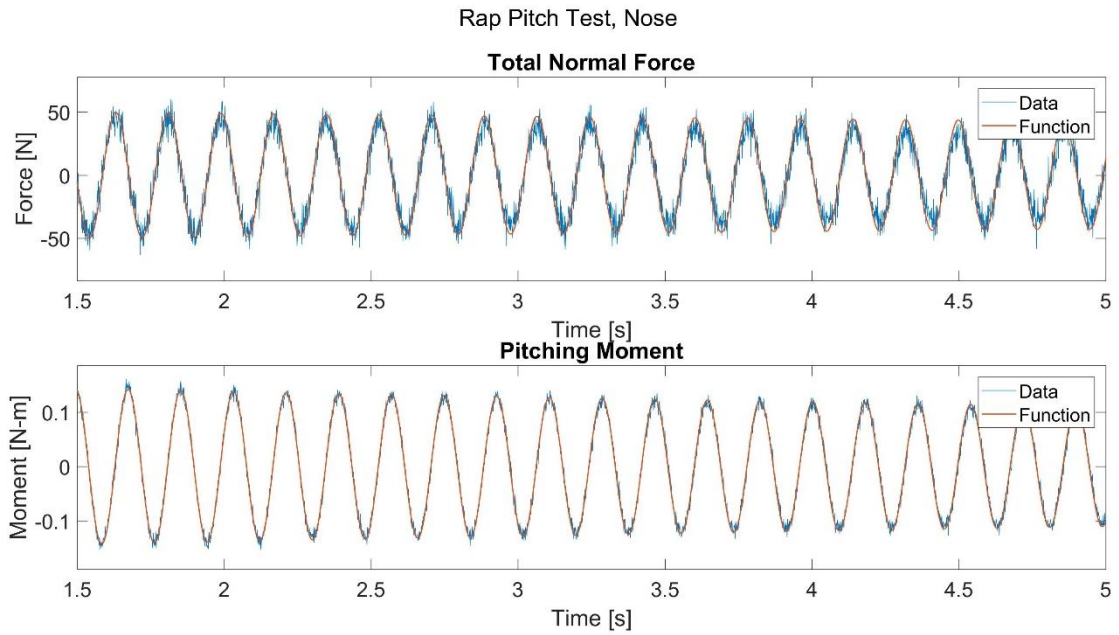
Figure 8. Underdamped Harmonic Oscillations Plotted on Top of the Response from the

Rap Pitch Test with Impulse at Nose.

Table 5. Values for Equation 16 for the Total Normal Force during Rap Pitch Tests.

Impulse Location	σ	ω (rad/s)	w_n (rad/s)	k (N/m)
Nose	0.045	35.06	35.06	88655
Center	0.065	35.09	35.09	88807
Tail	0.060	35.1	35.1	88858

Table 6. Values for Equation 16 for the Pitching Moment during Rap Pitch Tests.

Impulse Location	σ	ω (rad/s)	w_n (rad/s)	k (N/m)
Nose	0.075	35.06	35.06	88655
Center	0.065	35.1	35.1	88858
Tail	0.075	35.1	35.1	88858

The k_{NZ} term dominates the stiffness matrix. Therefore, the k_{NZ} value is calculated from the rap tests and used to calculate the rest of the stiffness matrix using the stiffness matrix equations in Chapter 4, shown in Equation 17. The k_{NZ} value is -888782 N/m and the length of the sting is 44 inches (0.12 meters). Using these values, EI is solved for and then plugged into the $k_{N\theta}$, k_{MZ}, and $k_{M\theta}$ expressions to get the values in Equation 18.

$$\begin{bmatrix} k_{NZ} & k_{N\theta} \\ k_{MZ} & k_{M\theta} \end{bmatrix} = \begin{bmatrix} -12EI/L^3 & -6EI/L^2 \\ 6EI/L^2 & 4EI/L \end{bmatrix} \tag{17}$$

$$\begin{bmatrix} k_{NZ} & k_{N\theta} \\ k_{MZ} & k_{M\theta} \end{bmatrix} = \begin{bmatrix} -88781.64 & -5766.38 \\ 5766.38 & 499.369 \end{bmatrix} \tag{18}$$

5.3   Initial Process Noise Covariance Estimate

The process noise covariance matrix, Q, represents how well the model predicts the process. Higher Q values mean that the model does an inadequate job at predicting the state. Consequentially, the range which the estimated state lies in is increased. A diagonal Q means that the state parameters are independent from each other. This is not true in this study since all the equations are coupled in the state space system. Therefore,

a fully populated, symmetric Q matrix is used for initial Kalman filtering. This is the Q prior to tuning the filter.

To calculate the Q, the variance of the difference between two runs at the same dynamic pressure and alpha were calculated. The variance for the z acceleration was used for the z position and velocity and the variance for the theta acceleration was used for the theta position and velocity. The variance for the normal force due to the internal balance was used for the aerodynamic normal force and the variance for the pitching moment due to the internal balance was used for the aerodynamic pitching moment. The square roots of the variances were calculated to yield the standard deviations and these were used as the diagonal of a process noise matrix. This matrix is multiplied by a matrix of normally distributed random numbers generated by the Matlab function "randn." Q is calculated by taking the covariance of the resulting matrix. Omidvarnia introduced this method in a simple example to explain how a linear Kalman filter works and how to implement the filter in Matlab. [9]

An illustration of the effectiveness of having a better initial estimate of the process noise covariance matrix is shown in Figure 9. The plot is an example of the residual for normal force due to the internal balance. As stated preciously, the residual is the difference between the measurements, y, and the observation model, Cx+Du. The objective is to minimize this residual. The blue line represents an estimate of the Q matrix with the diagonal equal to 10^{-5}. The red line uses Q with the method discussed above implemented. This shows that adjusting the Q matrix to be more representative of

the process noise dramatically reduces the residual. This also shows that the Q matrix is

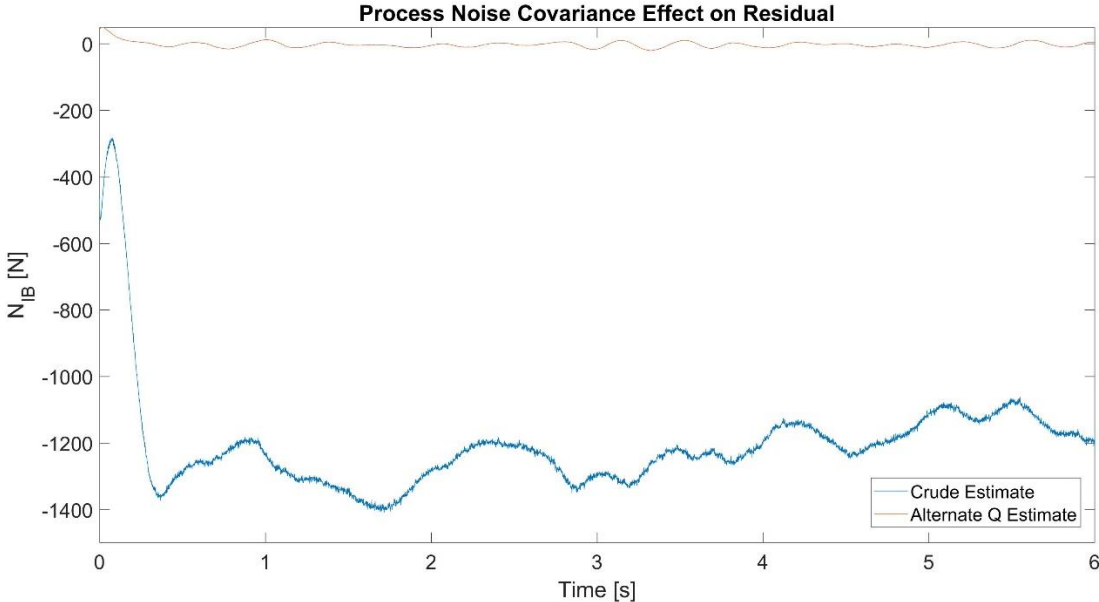essential to tuning the Kalman filter to get better convergence.

Figure 9. Effect of Estimation of Process Noise on the Residual.

CHAPTER VI

RESULTS

Carrying out the data analysis and constructing the Kalman filtering code allows all data points to be evaluated and their results interpreted. Results from three different techniques are illustrated below with explanations of data trends and the filtering performance. The first section discusses the results if the data was analyzed using the conventional method used at the LSWT. Follow-on sections examine the Kalman filter application for two state-space models.

6.1   Conventional Technique for Wind Tunnel Experimentation

Figure 10 is generated by using the current technique of time-averaging the data samples. Traditionally, the static tare tests remove the loads due to gravity to obtain the aerodynamic loads. The plot shown has the static tare values removed to show the aerodynamic loads for each dynamic pressure and angle of attack. An important feature that is missing from this plot is that it does not show that for each of the data points, the model is dynamic in the test section and the pitch angle is oscillating about the commanded angle of attack. As a result of the oscillations, the aerodynamic normal force is also changing with respect to time. This plot is used as a resource for checking the aerodynamic normal force output from the Kalman filter during the static rap tests.

For each dynamic pressure, the plots intersect at the same commanded angle of attack of -2°. As the dynamic pressure increases and the angle of attack increases, lift

increases as expected. For all dynamic pressures, the plots show stall at about 10°. Large oscillatory behavior of the model in the test section was observed at commanded angles above 10°. The oscillations were larger at higher dynamic pressures and commanded angles.

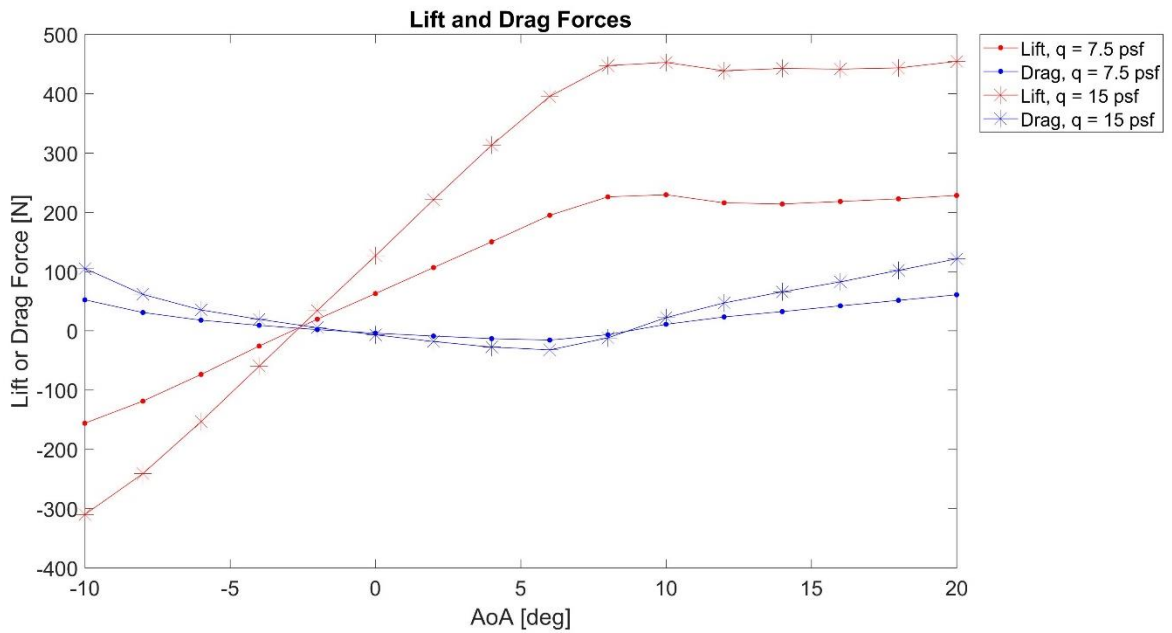
Figure 10. Summary Plot of Lift and Drag Forces Using Conventional Data Reduction Method.

6.2   Kalman Filter Results from 3-State Kalman Filter

The approach outlined in Chapters 4-6 using the collected data from the accelerometers and internal balance was attempted first using a 6-state model. However, the results showed large residuals and complications converging for the z acceleration

and theta acceleration. The troubleshooting and potential flaws of the system are explained below. A 3-state model did prove successful so is detailed first.

Simplifying the proposed model to one measurement and three state space variables proved successful for all data points. The internal balance normal force is the sole measurement with the plunge (z') position, plunge (z') velocity, and aerodynamic normal force as the state space variables. For the rap pitch test when θ_0 is zero, the output of the aerodynamic normal force matches the total lift calculated in Figure 10. Furthermore, the plunge (z') velocity and position oscillate about a reasonable value and with a minimum residual. These two characteristics were indicative of good performance of the filter using a simplified model. The appended test is explained below.

The state space model is simplified to a 3x3 matrix for A, a 3x1 matrix for B, and a 1x3 matrix for C. The simplified A, B, and C matrices are shown below. D is 0 because N_{IB} does not have any inputs.

$$u = \cos \theta_0$$

$$x_1 = z'$$

$$x_2 = \dot{z}'$$

$$x_3 = N_{aero}$$

$$\dot{x}_1 = \dot{z}' = x_2$$

$$\dot{x}_2 = \ddot{z}' = \frac{k_{NZ}g}{W} x_1 - \frac{g}{W} N_{aero} + gu$$

$$\dot{x}_3 = \dot{N}_{aero} = 0$$

Non-zero components of A matrix:

$$A_{1,2} = 1$$

$$A_{2,1} = \frac{k_{NZ}g}{W}$$

$$A_{2,3} = -\frac{g}{W}$$

Non-zero components of B:

$$B_{2,1} = g$$

Non-zero components of C:

$$C_{1,1} = k_{NZ}$$

The observability matrix is checked to confirm all states are observable. The rank of the observability matrix is 3 and the dimension of the state vector is 3. Therefore, all three states are observable with one measurement. The Kalman filter is implemented using the same Matlab code as the extended system except with the edited state space system and one measurement. The measurement error is 22.21 N^2. The process noise covariance matrix is a 3x3 matrix. Since the system is much simpler than before, only the diagonal is non-zero. For the first initial process noise matrix, the Q matrix is the identity matrix multiplied by 0.001.

To accelerate filter convergence, a better initial state estimate is used for the first time step. The initial condition for the state values is the steady-state plunge distance that the test article experiences due to the weight, 0 for plunge velocity, and an estimate for the aerodynamic normal force. The equations for the initial condition are shown below.

$$x_1(0) = \frac{(W - x_3(0))}{k_{NZ}}$$

$$x_2(0) = 0$$

$$x_3(0) = 2\pi \frac{AR}{AR + 2} qS \sin \theta_0$$

In order to improve filter convergence, a process called tuning is applied to the noise covariance matrices. To tune the filter, the diagonal of Q is modified. Increasing the element of the diagonal that multiplies that state value increases the process noise of that state value. Increasing the value is beneficial if process of calculating that state value is untrustworthy. If the process of calculating that state value is trusted, then lower process noise improves performance. The z' position and velocity have low process noise because their equations consider the bending of the sting and the aerodynamic normal force. As a result, the process of calculating the position and velocity displacement is more reliable.

The calculation of the aerodynamic normal force carries a larger process noise since multiple assumptions are made that contradict the model dynamics such as assuming the linear region of the lift curve slope and steady aerodynamic loads. First, even though the angle of attack of the model is not static, steady aerodynamics are assumed. Also, the time derivative of the aerodynamic normal force is shown in the state space model as not dependent on the pitch angle deflection, θ'. Therefore, the process noise must be larger for N_{aero}.

Another way to show that there needs to be a larger process noise for N_{aero} is to look at the reduced frequency value. The reduced frequency, defined $k = \omega c / U_\infty$,

characterizes the degree of unsteadiness of the flow. The equation for reduced frequency is shown below where ω is the natural frequency of the test article, c is the airfoil chord, and U_∞ is the freestream velocity. A crude estimate for the chord is the wingspan divided by the aspect ratio. For k=0, the flow is steady. For k between 0 and 0.05, the flow is quasi-steady and the unsteady effects can be neglected. For k greater than 0.05, flow is unsteady. For k greater than 0.2, flow is highly unsteady. The reduced frequencies for the dynamic pressures of 7.5, 15, and 22.5 psf are 1.19, 0.84, and 0.7 respectively. Because all reduced frequencies are greater than 0.2, the process noise for N_{aero} must be large since the unsteady effects are not included in the A matrix. [10]

Using the initial Q with the diagonal elements equal to 0.001, the results are shown for the state value estimates after applying the Kalman filter in Figure 11. These results are from a test case with the same dynamic pressure and angle of attack. On the same plot, the results from tuning the Q matrix are shown. Figure 12 shows the difference between the N_{IB} measurement and the predicted N_{IB} value resulting from the initial Q and the tuned Q. The goal is to minimize this difference. The goal is not achieved with the initial Q since the difference is steady at about 130 N. With the tuned Q, the residual is minimized. The tuned Q has a small process noise (0.001^2) corresponding to the z' position and z' velocity and a high process noise (100) corresponding to N_{aero}. The tuned Q is used for processing all configurations with the Kalman filter.
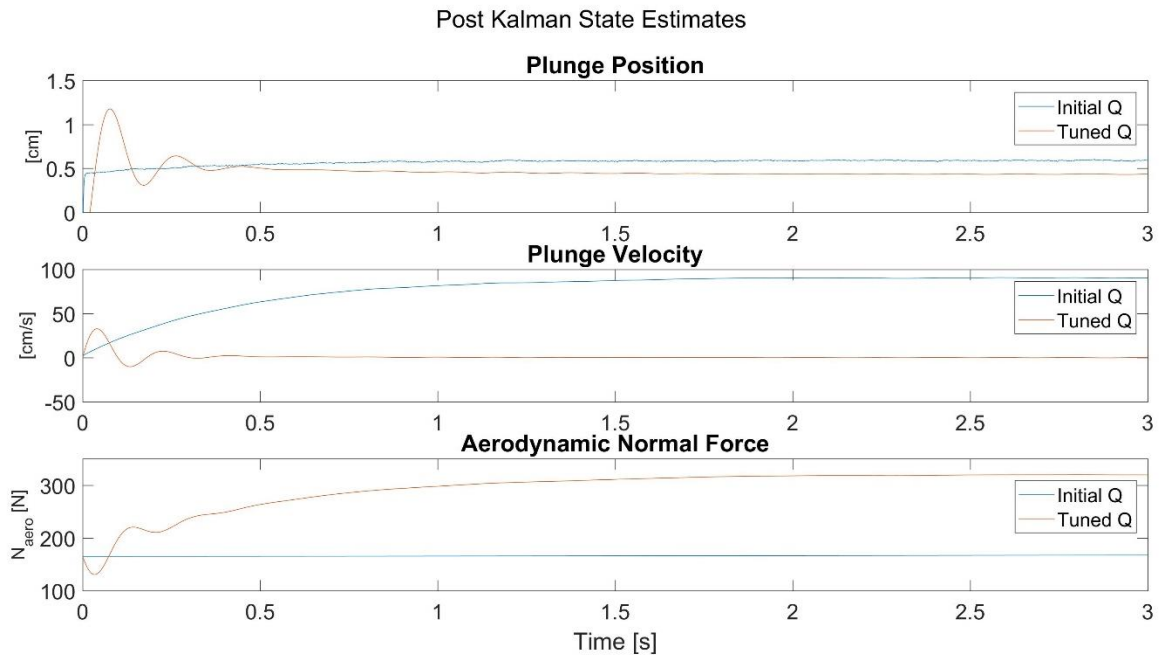
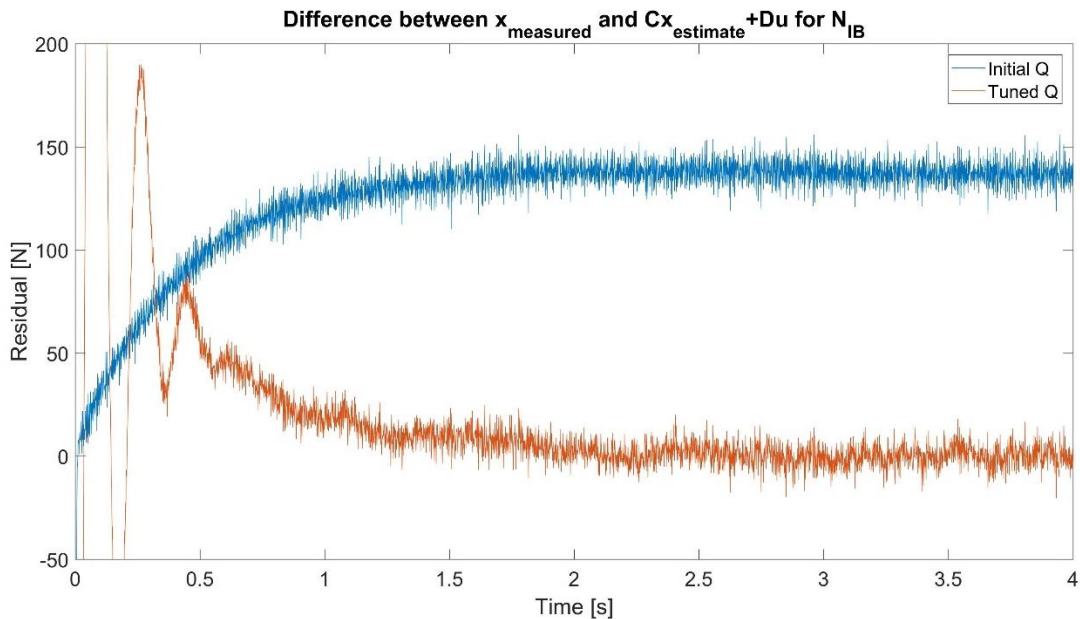*Figure 11. Post Kalman State Estimates Using Initial Q and Tuned Q.*

Figure 12. Difference Between Measurement and Estimated N_{IB} with Initial Q and Tuned Q.

First, the Kalman filter is applied to the rap tests with the wind off. A rubber mallet strikes the test article at three centerline locations. The first location is the nose, second is the center of the model, and the third is the tail of the model. The responses of rap tests are used to calculate the natural frequency of the test article. However, the Kalman filter is applied to the rap test data points in the interest of troubleshooting the filter and proving that the filter works since N_{aero} and M_{aero} should be roughly zero with wind-off. Results of executing the Kalman filter with the rap test with impulse at the nose is shown in Figure 13 and Figure 14 for the first 3 seconds. The large initial amplitude in blue on the plots in Figure 13 is from the impulse at the nose. After the impulse, the oscillations dampen out. The steady-state position of the test article is 0.8

49

cm below the zero position. This displacement is due to the weight of the test article. N_{aero} has the steady-state value of 0 N as predicted. In Figure 14, the initial amplitude for the Cx+Du plot in orange is due to the Kalman filter trying to lock onto the measured value of N_{IB} which takes less than a second. The second plot in Figure 14 mirrors the concept that the model can predict the measurement because after the model locks onto the measurement, the residual is approximately 0.
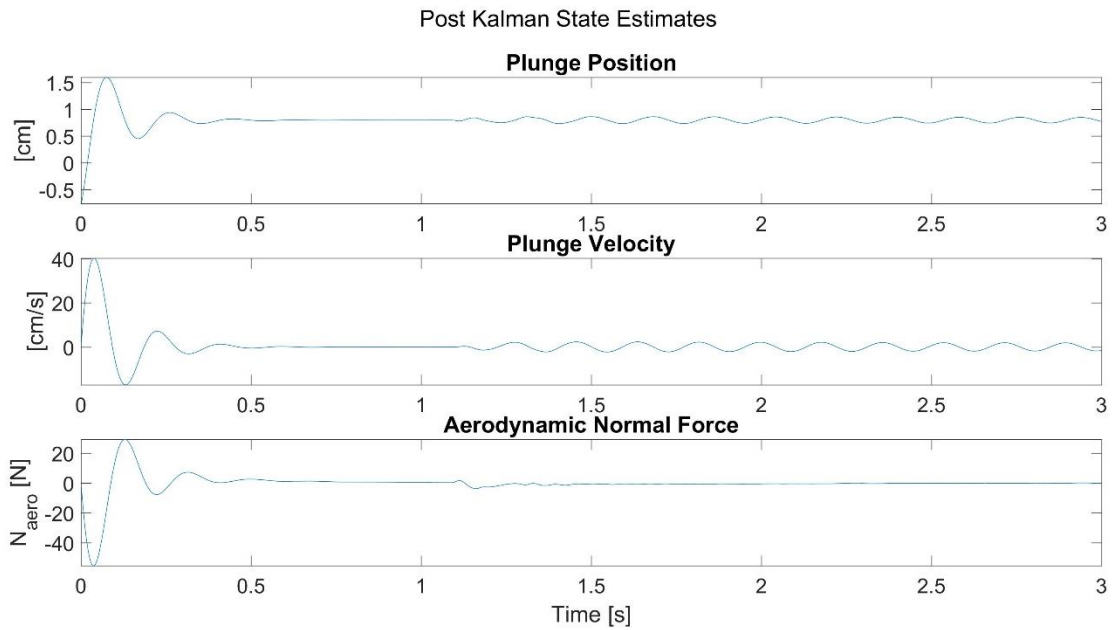

Figure 13. Post Kalman Estimates for Rap Pitch Test with Impulse at Nose.

Comparison of $x_{measured}$ and $Cx_{estimate}$+Du for N_{IB}
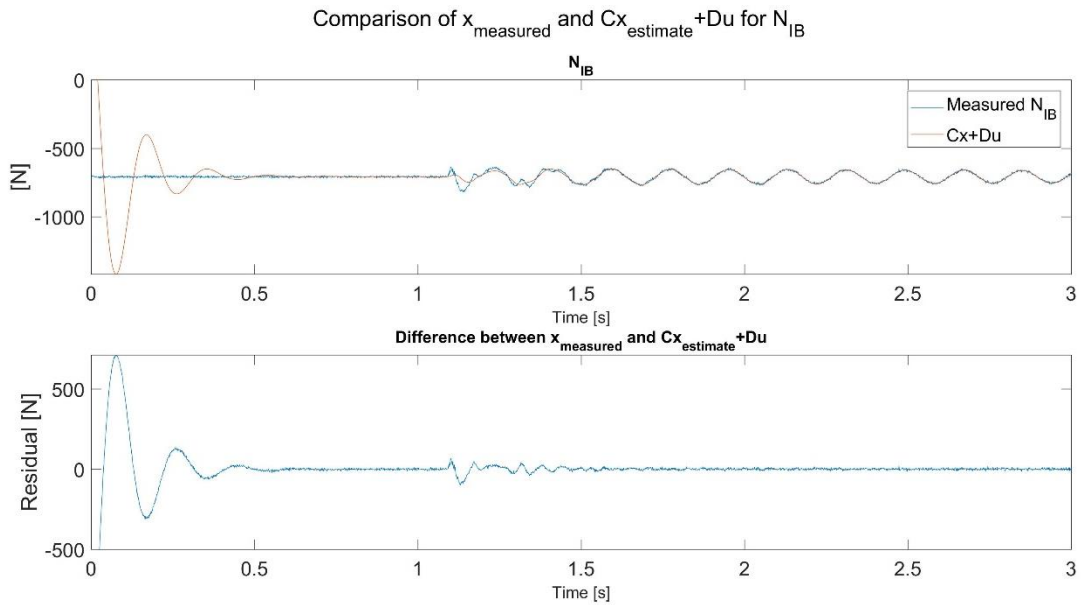
Figure 14. Comparison of Measurements with Predicted Measurements for Rap Pitch

Test with Impulse at Nose.

Another important feature to note is that the Kalman filter reduces the noise of the internal balance. This is shown in Figure 15 which shows a zoomed in view of the N_{IB} plot of Figure 14. The output is shown between 4 and 4.5 seconds. The blue line is the measurement with noise and the smooth orange line is the predicted measurement by the Kalman filter.

Figure 15. Example of Kalman Filter Reducing Noise in Measurement.

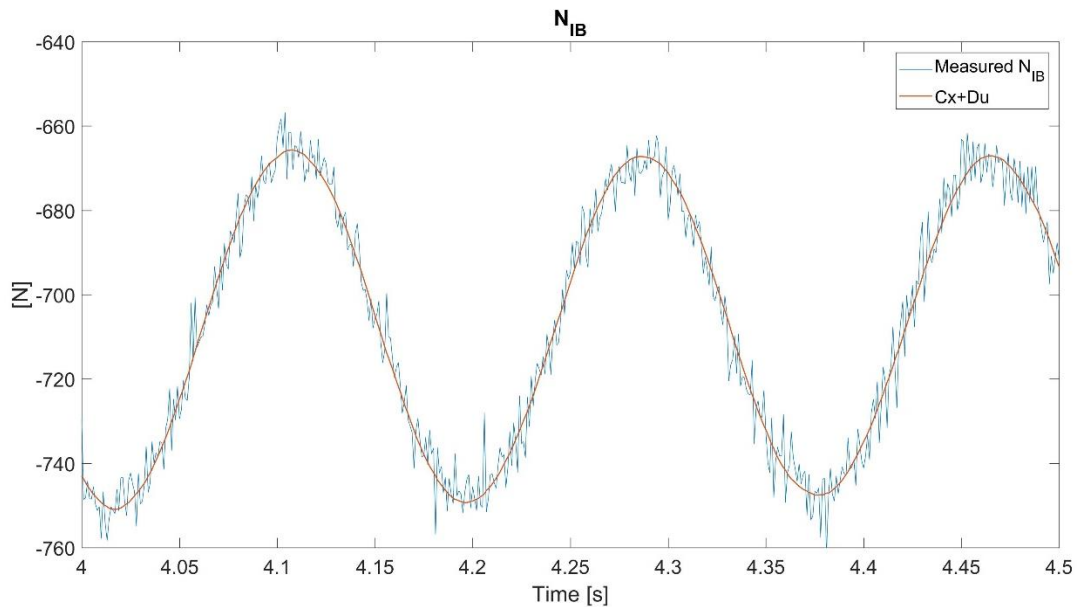The rap pitch test results show the dynamics of the model at a commanded pitch angle of 0° and wind-off. The next results discuss the effects of dynamic pressure and commanded pitch angle on the estimated position and aerodynamic load. The dynamic pressure and commanded angle of attack are changed as stated in Runs 15, 16, and 17 of Appendix A.

For the plots presented for the wind-on setting, the tuned Q is applied. For each of the three dynamic pressures, the state estimate from the Kalman filter and the NIB measurement and prediction comparison are plotted for three different commanded pitch angles. Figure 16 and Figure 17 show the results for the dynamic pressure of 7.5 psf, Figure 18 and Figure 19 show the results for 15 psf, and Figure 20 and Figure 21 show the results for 22.5 psf.
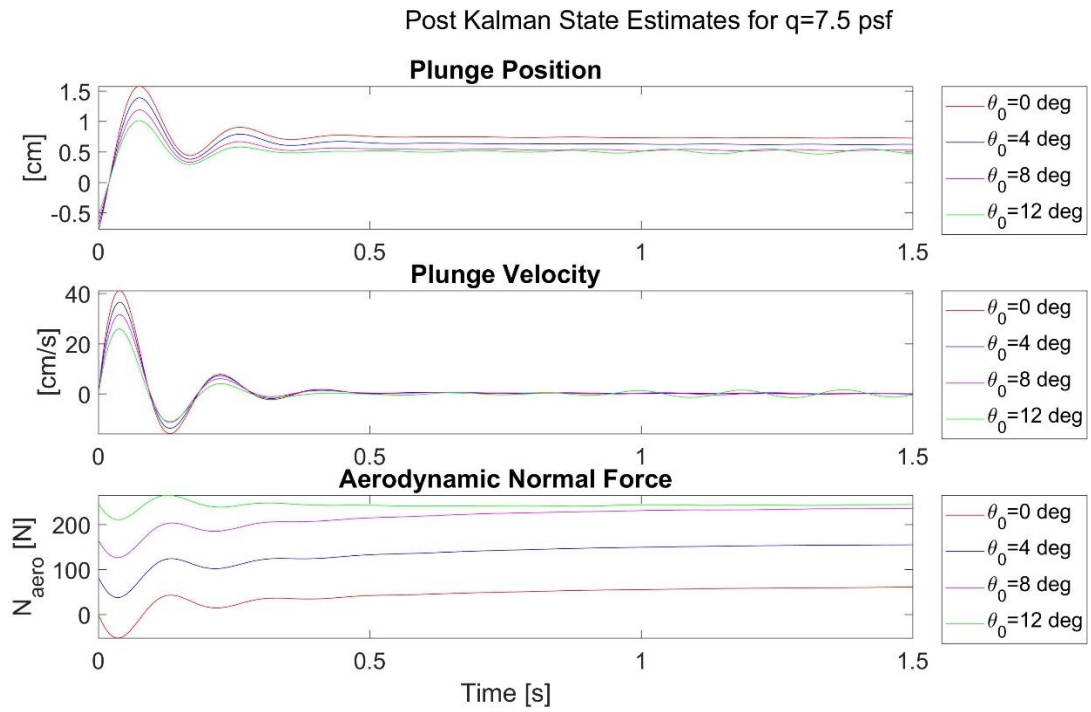
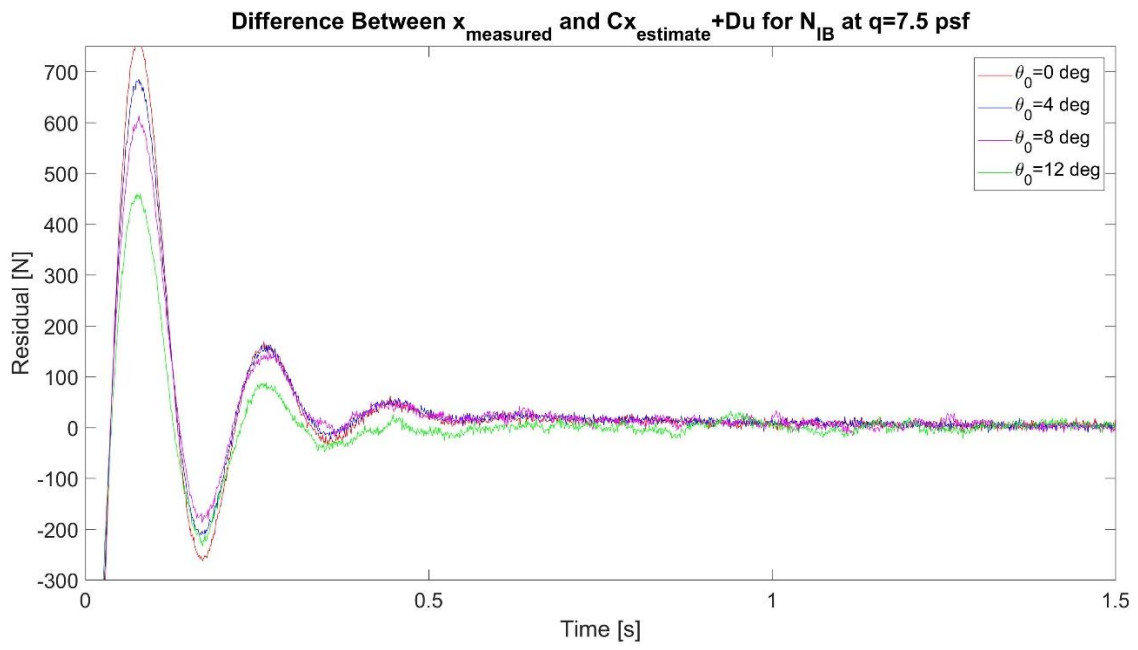*Figure 16. State Estimations for q=7.5 psf for a Variety of Pitch Angles.*

Figure 17. Residuals for a Variety of Pitch Angles at q=7.5 psf.
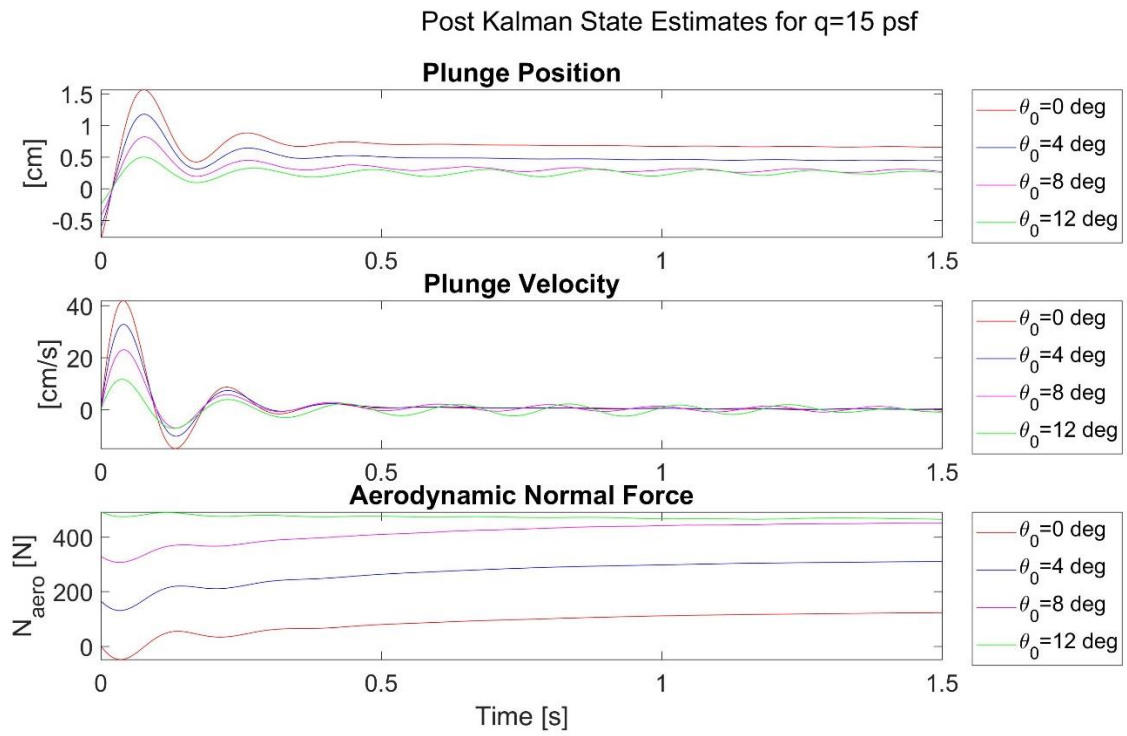
Figure 18. State Estimations for q=15 psf for a Variety of Pitch Angles.
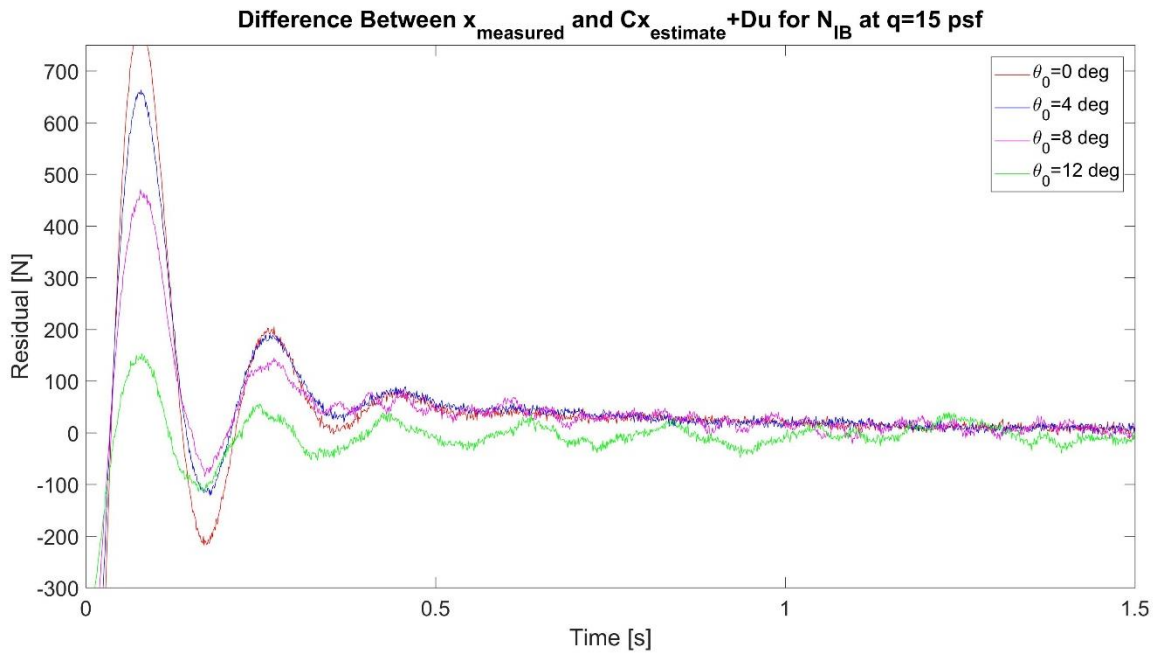
Figure 19. Residuals for a Variety of Pitch Angles at q=15 psf.
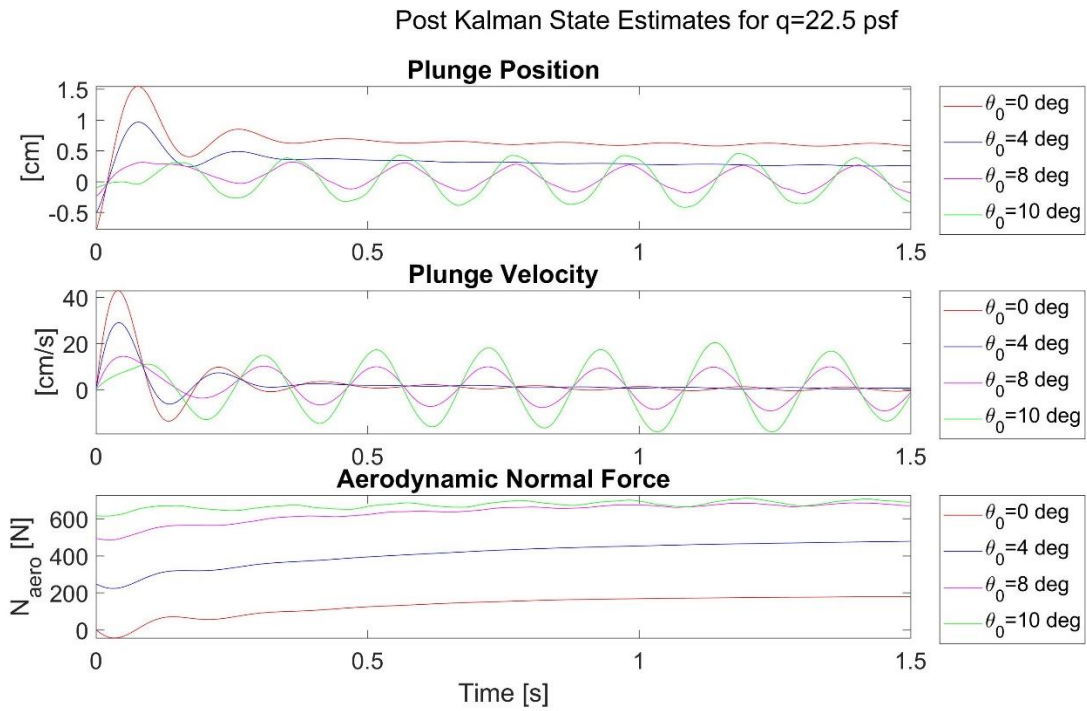
Figure 20. State Estimations for q=22.5 psf for a Variety of Pitch Angles.
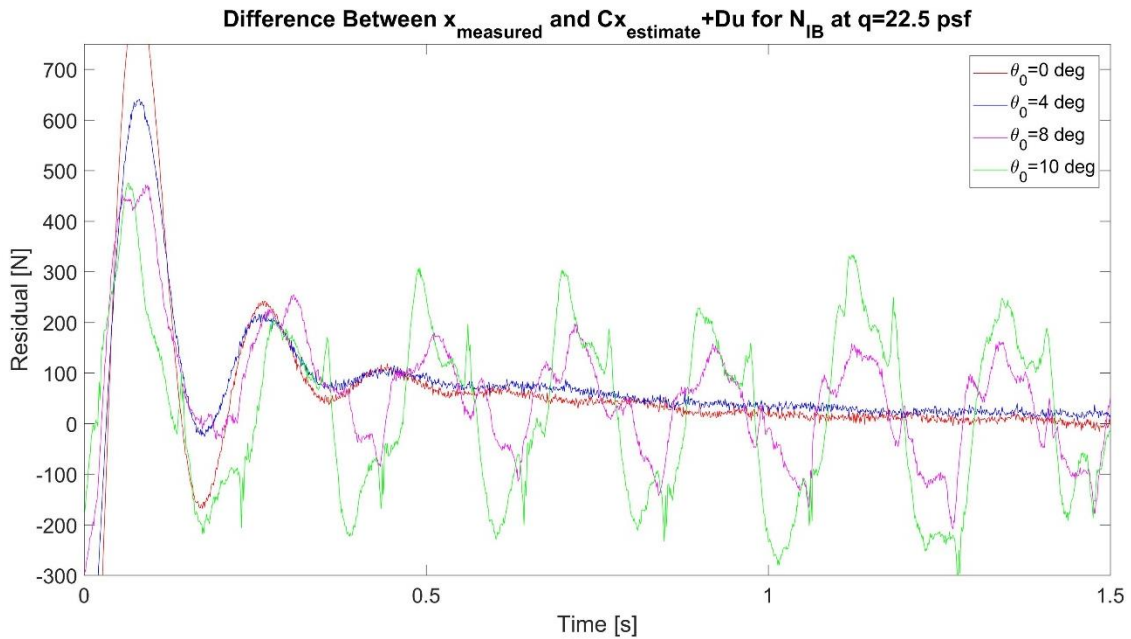
Figure 21. Residuals for a Variety of Pitch Angles at q=22.5 psf.

As the commanded pitch angle increases in all three dynamic pressure cases, the steady-state value of the plunge position decreases and oscillations increase in amplitude about the steady-state value. The decrease in plunge position is due to the increase in N_{aero}. N_{aero} increases and exhibits more oscillations as the commanded pitch angle increases and as the dynamic pressure increases. The plunge velocity oscillates about 0 in all cases. However, the amplitude of the plunge velocity increases as the commanded pitch angle increases. The sign of the plunge velocity is the opposite of the sign of the time derivative of N_{aero}. As the normal force increases (positive $d(N_{aero})/dt$), the velocity should be negative because the plunge below horizontal decreases as N_{aero} pushes the test article up.

57

Furthermore, the residual between the actual measurement and predicted measurement reaches the necessary steady-state value of 0 except in the θ_0=8 deg and θ_0=10 deg at q=22.5 psf cases. The reason for the larger residual is the test article reaches stall conditions. The Kalman filter output shows larger plunge oscillations for these cases, as was observed during the wind tunnel testing. The testing for q=22.5 psf was stopped at 10 degrees commanded pitch due to the large visible oscillations of the model. If the process noise is increased by orders of magnitude, the residual can be minimized by roughly 50% but does not reach a steady-state value of 0.

The 3-state Kalman filter results do not include the instantaneous pitch angle since only the plunge position and velocity and the aerodynamic normal force are estimated. To get an estimated value for the pitch angle, the term $\dot{z}'/U_\infty$ (plunge velocity divided by the freestream velocity) is added to the commanded pitch angle. For the dynamic pressure of 7.5 psf, the plunge velocity is reasonably small to assume a negligible correction to the instantaneous pitch angle. For the dynamic pressure of 15 psf, the largest correction to the commanded pitch angle is roughly 0.5° for the highest commanded pitch angle. At the highest dynamic pressure of 22.5 psf, the correction term ranges from 0.5° for θ=0° to 1.5° for θ=10°.

6.3   Kalman Filter Results from 6-State Kalman Filter

Before developing the 3-state estimator shown above, a full 6-state approach estimator was attempted. Tuning is the process of adjusting the values that affect the Kalman gain depending on whether the estimate needs to place more weight on the

measurements or the predictions. The filter will perform best if the measurement error is a true representation of the system. However, the process noise covariance matrix is generated by random noise making it difficult to initialize the Q matrix with true values. Therefore, the R matrix is held constant as the Q matrix is adjusted to achieve good filter performance.

The measurement covariance is calculated based on the known sensor noise and determines the variability in the measurements. Since the measurement error is known, the process noise is the main variable that is tuned to produce better performance of the Kalman filter and minimize the residual between the measurements and model. The code was first ran using a diagonal process noise covariance matrix and tuned by increasing or decreasing the numbers on the diagonal. This method produced a large residual for all parameters and the filter did not converge during the 20 second time sample. Implementing the method discussed in Section 5.3 produced better results with the residual near zero for the normal force due to the internal balance. However, the plunge (z') acceleration and pitch (θ') acceleration proved difficult to minimize the residual between the measurement and model prediction.

Not only was the residual large, but the behavior of the state values after applying the Kalman filter exhibited large values for the plunge and pitch velocities as well as the aerodynamic normal force and pitching moment showing an increasing linear relationship. All plots should be demonstrating small oscillations about 0. The behavior of individual plots improved by tuning the filter, however, changing the individual elements of the Q matrix is very tedious. The Q matrix has 36 values that can be tuned.

Changing one of the elements on the off-diagonal influenced multiple state values since the equations are coupled. Changing the values on the diagonal changes the process noise of that state value. Unfortunately, solely changing the diagonal values was not sufficient to achieve filter convergence.

A potential reason for the difficulty in tuning the z' acceleration and θ' acceleration is the large amount of noise produced by the accelerometers. For this reason, during the system identification process, the strain gauge output was used to quantify the natural frequency and stiffness coefficients instead of the accelerometers. The accelerometers may not have been mounted sufficiently to reduce any vibrations transmitting from the model to the accelerometers. The excessive noise seen in the accelerometer readings as shown in Figure 22 may be vibration from insufficient mounting coupled with the oscillations of the model. The plunge acceleration shows less noise than the pitch angular acceleration. The pitch angular acceleration also shows large oscillations at roughly ±100 deg/s^2 amplitudes. Figure 22 and Figure 23 are responses to the rap pitch test with the impulse applied at the nose of the model. These data points had the wind off with only the impulse force imparted on the model, yet the acceleration response showed large noise variations
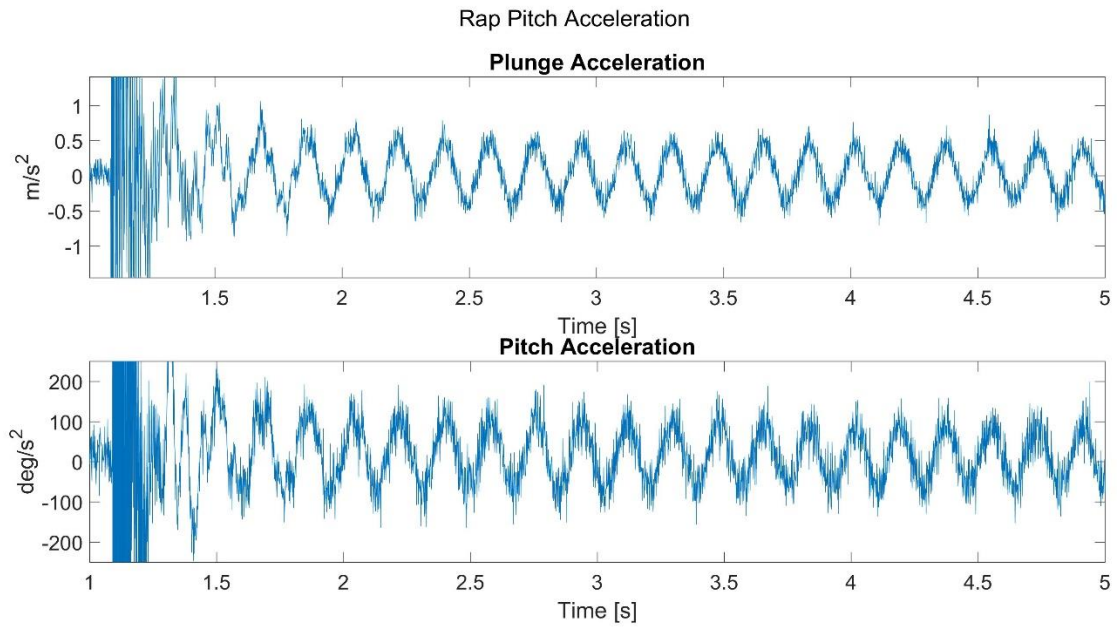
Rap Pitch Acceleration

Figure 22. Plunge (z') and Pitch (θ') Acceleration Response for Rap Pitch Nose.
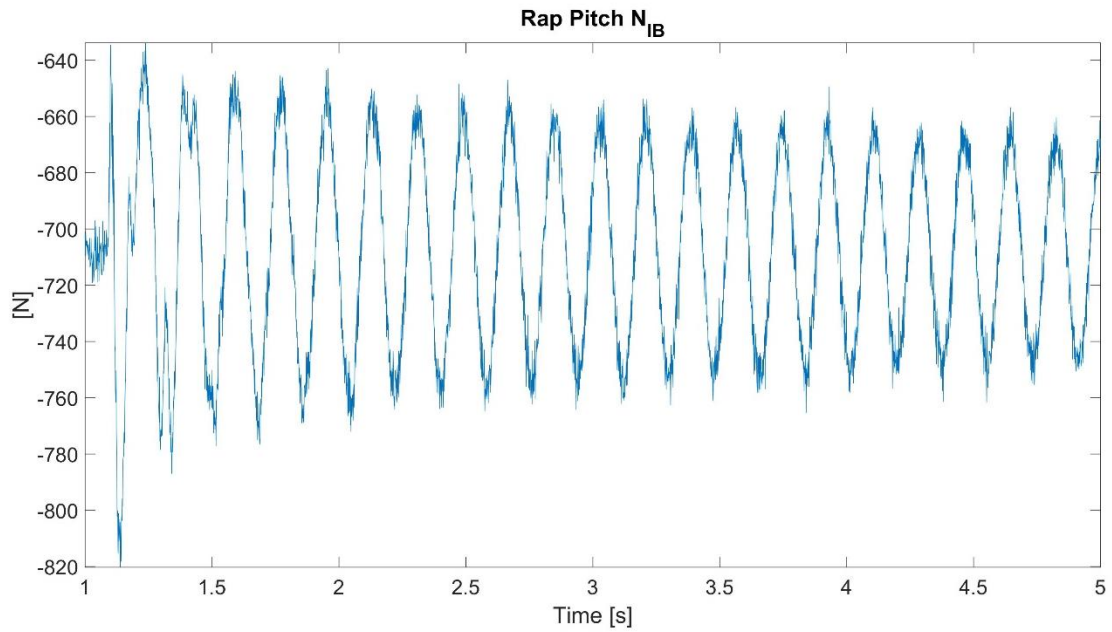
Figure 23. Normal Force due to Internal Balance Response for Rap Pitch Nose.

61

6.3.1 Continued Troubleshooting

In an effort to build upon the 3-state Kalman filter model that has been proven successful, the z accelerometer data is added as a second measurement to the Kalman filter. Adding this measurement changes the C and D matrices and these matrices are defined below. C is a 2x3 matrix and D is a 2x1 matrix.

Non-zero components of C matrix:

$$C_{1,1} = \frac{k_{NZ} g}{W}$$

$$C_{1,3} = -\frac{g}{W}$$

$$C_{2,1} = k_{NZ}$$

Non-zero components of D matrix:

$$D_1 = g$$

Unfortunately, the plunge velocity and aerodynamic normal force exhibited the same behavior as the extensive state space model that was initially introduced in Chapter 4. The estimated plunge velocity plot showed exponentially large velocities that were not feasible. The estimated N_{aero} displayed an increasing linear relationship, whereas in the 3-state model, N_{aero} had an oscillatory response about a steady state value that was similar to the value in Figure 10.

CHAPTER VII

CONCLUSIONS

The goal of this thesis was to prove successful utilization of the Kalman filter technique in test article state estimation so that future wind tunnel test events can follow this approach for efficiency and data accuracy.

To achieve the fundamental goal, a state space model that represents the motion of a sting-mounted wind tunnel model was constructed and data was collected from accelerometers and the internal balance. The Kalman filter was applied to the wind tunnel measurements using the state space model and tuned to achieve favorable performance. During this process, several observations were made.

First, the extended state space system that included pitch and plunge motion plus normal force, pitch moment, and acceleration data did not demonstrate good performance due to the complexity of tuning the process noise covariance matrix. The residual between measurements and the predicted measurements was minimized for 1 of the 4 measurements. Attempts at tuning the other parameters led to flawed state estimate results. All state space equations are coupled and experience process noise from multiple state space variables. The Autocovariance Least-Squares (ALS) technique might improve this situation. To overcome this problem, the model was simplified to three state space variables and the normal force due to the internal balance as the sole measurement.

Results from the simplified model indicate that the Kalman filter is beneficial to quantifying the plunge motion of the test article as well as the oscillations in the aerodynamic normal force. Furthermore, tuning the filter by adjusting Q is essential to achieving convergence of the Kalman filter. After attaining optimal performance, multiple trends were conclusive regarding the state estimates and system noise. As the commanded pitch angle increases, the plunge position decreases because the aerodynamic normal force increases. At the same time, the state estimate responses exhibit larger amplitudes at larger pitch angles and becomes more apparent with larger dynamic pressures. At stall conditions, the filter still behaves nominally but the residual and amplitude oscillations increase substantially.

For testing at the LSWT, it is not recommended to use the Kalman filter during stall conditions or if the process noise must be larger than 100 units to minimize the residual. Also, if the residual cannot be minimized less than a threshold relative to the measurement, the filter is not suitable to produce trustworthy results. The last recommendation is to ensure fixed mounting of the accelerometers to the test article to reduce noise and external vibrations transmitted to the model. For future tests, the LSWT team will only need to change parameter values and conduct the system identification tests to implement the Kalman filter for state estimation.

During the course of data acquisition and state estimation, multiple improvements became apparent for future work. An important issue during the test was the accelerometer noise. The noise was apparent during the simple rap tests. Due to the noise, N_{IB} output had to be used for system identification instead of the accelerometer

data. In future tests, accelerometers with less noise or higher sensitivity are recommended. Another improvement, rather than different accelerometers, is to ensure a more robust way to mount the accelerometers that will reduce any extra vibration.

Tuning the filter was an important step to getting the optimum estimation and smallest residual. For the extended state space system, tuning the Q matrix was burdensome. After calculating an initial Q, the matrix had to be hand-tuned by changing individual elements to slightly larger or smaller values to minimize the residual. In the future, a better technique like the ALS technique for tuning the Kalman filter by finding the best P and Q matrices would decrease the time required to implement this state estimation approach in wind tunnel testing.

Valasek and Chen use the Observer/Kalman Filter Identification (OKID) technique to complete the system identification process an alternate way than the technique displayed here [11]. The technique could be used instead of the current practice in this work to identify the linear dynamic model of a nonlinear system. Applying the OKID method to this test would be useful to compare the OKID results with the present results and determine which technique would be more beneficial and robust for wind tunnel testing. This technique would eliminate the a priori assumptions about the model structure. For the present research, OKID was not used because there is value in deriving and understanding the forces and moments acting upon the test article and sting system.

Furthermore, the current test focused on the pitch motion of the test article. Upon successful completion of the extended state space system, future tests can focus on the

roll and yaw motion of the test article. Accelerometers can be mounted on the wing tips to calculate the roll and yaw parameters. This test focused on one degree of freedom since adding more degrees of freedom would increase the complexity of the state estimation and tuning.

REFERENCES

1. Crassidis, J. L., and Junkins, J. L., 2011. *Optimal Estimation of Dynamic Systems*, 2nd ed. Taylor and Francis, New York.

2. Crawford, B. L. and Finley, T. D., "Results from a Sting Whip Correction Verification Test at the Langley 16-Foot Transonic Tunnel," AIAA 2002-0879, 40th AIAA Aerospace Sciences Meeting & Exhibit, 14-17 January 2002, Reno, NV.

3. Steinle, Frank W., Jr. and Peters, William L., "Processing Balance Data to Determine True Static Aerodynamic Forces and Moments," AIAA 2007-5327, 43rd AIAA/ASME/SAE/ASEE Joint Propulsion Conference and Exhibit, 8-10 July, Cincinnati, OH.

4. Weiss J., "Model Vibrations and Inertial Bias Measurement in a Transonic Wind Tunnel Test," AIAA 2008-4033, 26th AIAA Aerodynamic Measurement Technology and Ground Testing Conference. 23-26 June 2008.

5. Maybeck, P. S. and Siouris, G. M., "Stochastic Models, Estimation, and Control, Volume I," *IEEE Transactions on Systems, Man, and Cybernetics*, vol. 10, no. 5, pp. 282-282, May 1980. doi: 10.1109/TSMC.1980.4308494

6. Rajamani, M. R., and Rawlings, J. B., 2009. "Estimation of the disturbance structure from data using semidefinite programming and optimal weighting". *Automatica*, 45(1), pp. 142–148.

7. "WB-57 High Altitude Research." *NASA/JSC Aircraft Operations*, NASA, 20 Oct. 2017, jsc-aircraft-ops.jsc.nasa.gov/wb57/performance.html.

8. Kleinbauer, Rachel, "Kalman Filtering Implementation with MatLab," University Stuttgart Institute of Geodesy, Helsinki, November 2004.

9. Omidvarnia, Amir. "Linear Kalman Filter." *File Exchange*, MathWorks, 24 Nov. 2010, www.mathworks.com/matlabcentral/fileexchange/29127-linear-kalman-filter.

10. Leishman, J G. *Principles of Helicopter Aerodynamics.* Cambridge: Cambridge University Press, 2006. Print.

11. Valasek, John, and Chen, Wei, "Observer/Kalman Filter Identification for On-Line System Identification of Aircraft," *Journal of Guidance, Control, and Dynamics,* Volume 26, Number 2, pp. 347-353, March-April 2003.

Conventional Sting Deflection				
Test	**Run**	**Point**	**Description**	**Comments**
1707	13	1	Static	
Rap Tests, Wind Off, Strike with Mallet at 3 Locations				
Test	**Run**	**Point**	**Description**	**Comments**
1707	13	2	Rap Pitch – Nose	
1707	13	3	Rap Pitch – Center	
1707	13	4	Rap Pitch – Tail	
1707	13	5	Rap Roll – Port Wing Tip	Capping max amount of accelerometer; with regards to sensitivity and range, probably not the right accelerometers
1707	13	6	Rap Roll – Center	
1707	13	7	Rap Roll – Starboard Wing Tip	Capping max amount of accelerometer; with regards to sensitivity and range, probably not the right accelerometers
1707	13	8	Rap Yaw – Port Side of Nose	
1707	13	9	Rap Yaw – Trailing Edge of Port Wing	
1707	13	10	Rap Yaw – Starboard Side of Tail	One wing's accelerometer is capping max

Test	Run	Point	Description	Comments
1707	13	11	Rap Roll – Using Hand	Bad data
1707	13	12	Rap Roll – Using Hand	Retry of Point 11, Good data

Conventional Static Tare Pitch Sweep				
Test	**Run**	**Point**	**Description**	**Comments**
1707	14	1	Static Tare, α=0°	Balance data should be the same at points 7 and 18
1707	14	2	Static Tare, α=-10°	
1707	14	3	Static Tare, α=-8°	
1707	14	4	Static Tare, α=-6°	
1707	14	5	Static Tare, α=-4°	
1707	14	6	Static Tare, α=-2°	
1707	14	7	Static Tare, α=0°	Balance data should be the same at points 1 and 18
1707	14	8	Static Tare, α=2°	
1707	14	9	Static Tare, α=4°	
1707	14	10	Static Tare, α=6°	
1707	14	11	Static Tare, α=8°	
1707	14	12	Static Tare, α=10°	
1707	14	13	Static Tare, α=12°	
1707	14	14	Static Tare, α=14°	
1707	14	15	Static Tare, α=16°	
1707	14	16	Static Tare, α=18°	
1707	14	17	Static Tare, α=20°	

Test	Run	Point	Description	Comments
1707	14	18	Static Tare, α=0°	Balance data should be the same at points 1 and 7
Single α Runs at q=7.5 psf with Accelerometers and Internal Balance				
Test	**Run**	**Point**	**Description**	**Comments**
1707	15	1	α=0°, wind off	
1707	15	2	α=0°, wind on, q=7.5 psf	
1707	15	3	α=-10°, wind on, q=7.5 psf	
1707	15	4	α=-8°, wind on, q=7.5 psf	
1707	15	5	α=-6°, wind on, q=7.5 psf	
1707	15	6	α=-4°, wind on, q=7.5 psf	
1707	15	7	α=-2°, wind on, q=7.5 psf	
1707	15	8	α=0°, wind on, q=7.5 psf	
1707	15	9	α=2°, wind on, q=7.5 psf	
1707	15	10	α=4°, wind on, q=7.5 psf	
1707	15	11	α=6°, wind on, q=7.5 psf	
1707	15	12	α=8°, wind on, q=7.5 psf	
1707	15	13	α=10°, wind on, q=7.5 psf	
1707	15	14	α=12°, wind on, q=7.5 psf	
1707	15	15	α=14°, wind on, q=7.5 psf	
1707	15	16	α=16°, wind on, q=7.5 psf	
1707	15	17	α=18°, wind on, q=7.5 psf	
1707	15	18	α=20°, wind on, q=7.5 psf	

Test	Run	Point	Description	Comments
1707	15	19	α=0°, wind on, q=7.5 psf	
Single α Runs at q=15 psf with Accelerometers and Internal Balance				
Test	**Run**	**Point**	**Description**	**Comments**
1707	16	2	α=0°, wind on, q=15 psf	
1707	16	3	α=-10°, wind on, q=15 psf	
1707	16	4	α=-8°, wind on, q=15 psf	
1707	16	5	α=-6°, wind on, q=15 psf	
1707	16	6	α=-4°, wind on, q=15 psf	
1707	16	7	α=-2°, wind on, q=15 psf	
1707	16	8	α=0°, wind on, q=15 psf	
1707	16	9	α=2°, wind on, q=15 psf	
1707	16	10	α=4°, wind on, q=15 psf	
1707	16	11	α=6°, wind on, q=15 psf	
1707	16	12	α=8°, wind on, q=15 psf	
1707	16	13	α=10°, wind on, q=15 psf	
1707	16	14	α=12°, wind on, q=15 psf	
1707	16	15	α=14°, wind on, q=15 psf	
1707	16	16	α=16°, wind on, q=15 psf	
1707	16	17	α=18°, wind on, q=15 psf	
1707	16	18	α=20°, wind on, q=15 psf	
1707	16	19	α=0°, wind on, q=15 psf	

Single α Runs at q=22.5 psf with Accelerometers and Internal Balance				
Test	**Run**	**Point**	**Description**	**Comments**
1707	17	2	α=0°, wind on, q=22.5 psf	
1707	17	3	α=2°, wind on, q=22.5 psf	
1707	17	4	α=4°, wind on, q=22.5 psf	
1707	17	5	α=6°, wind on, q=22.5 psf	
1707	17	6	α=8°, wind on, q=22.5 psf	
1707	17	7	α=10°, wind on, q=22.5 psf	Too dynamic, HARS showed movement
1707	17	8	α=0°, wind on, q=22.5 psf	
1707	17	9	α=0°, wind off	

APPENDIX B

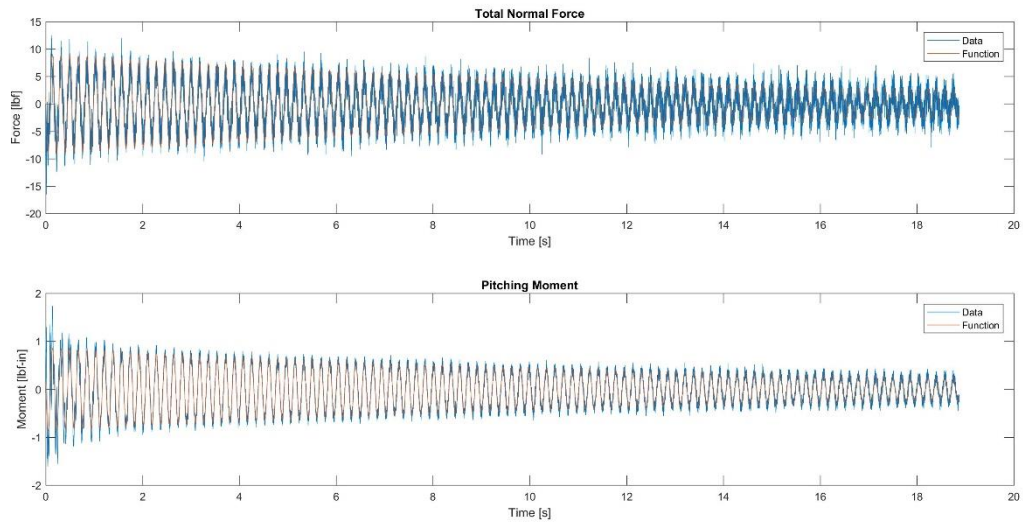## RAP PITCH SYSTEM IDENTIFICATION TEST RESPONSES

Rap Pitch Test, Nose
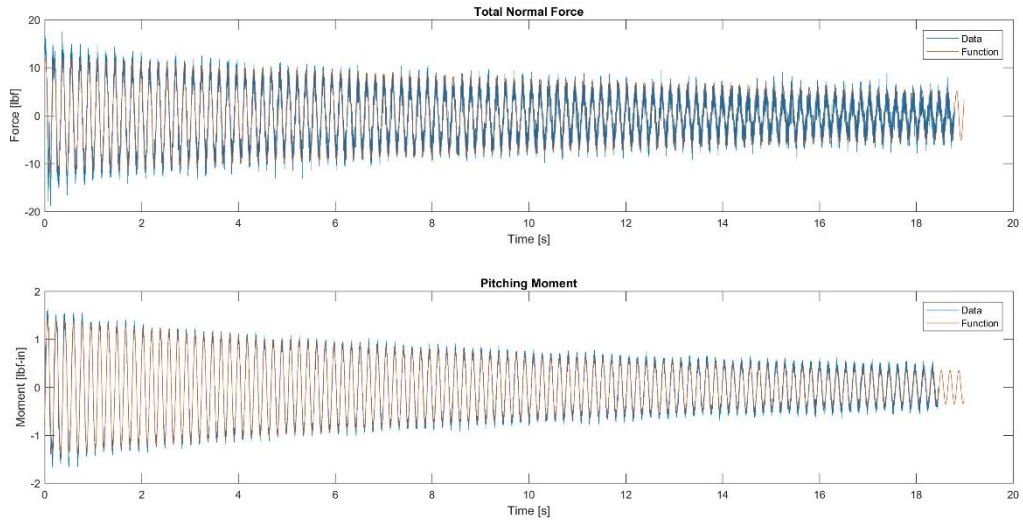
Rap Pitch Test, Center

Rap Pitch Test, Tail